Long-range transport of stratospheric aerosols in the Southern Hemisphere following the 2015 Calbuco eruption

Nelson Bègue[1], Damien Vignelles[2], Gwenaël Berthet[2], Thierry Portafaix[1], Guillaume Payen[1], Fabrice Jégou[2], Hassan Benchérif[1,6], Julien Jumelet[3], Jean-Paul Vernier[4], Thibaut Lurton[2], Jean-Baptiste Renard[2], Lieven Clarisse[5], Vincent Duverger[2], Françoise. Posny[1], Jean-Marc Metzger[1] and Sophie Godin-Beekmann[3]

[1] Laboratoire de l'Atmosphère et des Cyclones, UMR 8105 CNRS, Université de la Réunion, Reunion Island, France.

[2] Laboratoire de Physique et Chimie de l'Environnement et de l'Espace, Université d'Orléans, CNRS/INSU UMR7328, Orléans, France

[3] Laboratoire Atmosphère Milieux Observations Spatiales, University of Paris VI, Paris, France

[4] NASA Langley Research Center, Hampton, Virginia, USA

[5] Spectroscopie de l'Atmosphère, Service de Chimie Quantique et Photophysique, Université Libre de Bruxelles, Brussels, Belgium

[6] School of Chemistry and Physics, University of KwaZulu-Natal, Westville, Durban, South Africa

Correspondence to: N.Bègue (nelson.begue@univ-reunion.fr)

Abstract

After 43 years of inactivity, the Calbuco volcano which is located in the southern part of Chile erupted on 22 April 2015. The space-time evolutions (distribution and transport) of its aerosol plume are investigated by combining satellite (CALIOP, IASI, OMPS), in situ aerosol counting (LOAC OPC) and LiDAR observations, and the MIMOSA advection model. The Calbuco aerosol plume reached the Indian Ocean one week after the eruption. Over the Reunion Island site (21°S; 55.5°E), the aerosol signal was unambiguously enhanced in comparison with "background" conditions with a volcanic aerosol layer extending from 18 km to 21 km during the May-July period. All the data reveal an increase by a factor of ~2 in the sAOD (stratospheric Aerosol Optical Depth) with respect to values observed before the eruption. The aerosol mass e-folding time is approximately 90 days which is rather close to the value (~80 days) reported

for the Sarychev eruption. Microphysical measurements obtained before, during and after the eruption reflecting the impact of the Calbuco eruption on the lower stratospheric aerosol content have been analyzed over the Reunion Island site. During the passage of the plume, the volcanic aerosol was characterized by an effective radius of 0.16 ±0.02 µm with a unimodal size distribution for particles above 0.2 µm diameter. Particle concentrations for sizes larger than 1 µm are too low to be properly detected by the LOAC OPC. The aerosol number concentration was ~20 times higher that observed before and one year after the eruption. According to OMPS and LiDAR observations, a tendency toward conditions before the eruption has been observed by April 2016. The volcanic aerosol plume is advected eastward in the Southern Hemisphere and its latitudinal extent is clearly bounded by the subtropical barrier and the polar vortex. The transient behavior of the aerosol layers observed above Reunion Island between May and July 2015 reflects an inhomogeneous spatio-temporal distribution of the plume which is controlled by the localization of these dynamical barriers.

1. Introduction

Stratospheric aerosols affect the chemical and radiation balance of the atmosphere (McCormick et al., 1995; Solomon, 1999; SPARC 2006). The importance of stratospheric aerosols on the chemistry is mostly due to its role in the ozone budget (Solomon et al., 1986; Bekki, 1997; Borrmann et al., 1997). Stratospheric aerosols provide sites for heterogeneous chemical reactions leading to stratospheric ozone depletion, significantly enhanced in periods of high aerosol loadings following major volcanic eruptions (Solomon, 1999 and references therein). In addition, periods of enhanced stratospheric aerosols loadings can lead to significant warming in the stratosphere and cooling in the troposphere (e.g. McCormick et al., 1995; Solomon et al., 2011; Arfeuille et al., 2013). As reported by Kremser et al. (2016), a better understanding of the processes governing the lifetime of stratospheric aerosols are needed to assess the impacts on climate and chemistry. Since the discovery of the permanent stratospheric aerosol layer, called Junge Layer, in 1961 (Junge, 1961), it has been established that stratospheric aerosols are mostly composed of sulfuric acid droplets with some more complex characteristics in the stratosphere where organic compounds and meteoritic dust can also contribute to its composition (Froyd et al., 2009; Mossop, 1965; Murphy et al., 1998). The main sources of stratospheric sulfur are Carbonyl Sulfide (OCS), Dimethyl Sulfide (DMS) and sulfur dioxide (SO_2) (SPARC, 2006), the latter being significantly enhanced after volcanic eruptions (Carn et al., 2015). The injected SO_2 into stratosphere is oxidized into H_2SO_4, which (after homogeneous nucleation and/or condensation onto existing aerosol particles) causes an increase in the content

of liquid sulfate aerosol (SPARC, 2006). Based on the control of the stratospheric aerosols burden over the last 25 years, Thomason et al. (2007) showed that volcanic effects dominate over natural and anthropogenic sources. Previous studies on stratospheric aerosols have significantly characterized its properties and variability during "background" (i.e. free of volcanic aerosols) and volcanic conditions (e.g., Stenchikov et al., 1998; Jäger and Deshler, 2002; Bauman et al., 2003; Hermann et al; 2003; Hofmann et al; 2009).

The eruption of Pinatubo in 1991 is known to be the last major volcanic eruption injecting between 14 and 23 Tg of SO_2 significantly perturbed the global stratosphere for several years (Kinninson et al., 1994; McCormick et al., 1995; Stenchikov et al., 1998, 2002; Guo et al., 2004; Dhomse et al., 2014). As reported by Russell et al. (1996), in addition to the prodigious increase in the stratospheric aerosols loading, this event significantly affected numerous aspects of the atmospheric system including: i) a 2-year cooling of the global surface temperature of several tenths of degrees (Canty et al., 2013; Wunderlich and Mitchell, 2017); ii) a warming of the tropical stratosphere ranging from 1° to 4°C (Labitzke and McCormick et al., 1992; Young et al., 1994); (iii) a lifting of the tropical ozone layer by ~1.8 km (Pueschel et al., 1992; Grant et al., 1994). By the use of satellite and balloon-borne observations, various studies have shown that moderate volcanic eruptions (i.e., volcanic explosive index less or equal to 4) can significantly modulate stratospheric aerosols concentrations (Bourassa et al., 2010; Kravitz et al., 2010; Solomon et al., 2011; Vernier et al., 2011; Clarisse et al., 2012; Jégou et al., 2013). Based upon satellite observations, Vernier et al (2011) showed that the decadal increase in stratospheric aerosol loadings since 2002 can be attributed to a series of moderate volcanic eruptions. As reported by Kremser et al (2016), this decadal trend was also obtained from LiDAR (Hofmann et al., 2009; Trickl et al., 2013; Zuev et al., 2017) and ground-based sun-photometer observations (Ridley et al., 2014). Three moderate volcanic eruptions occurred in the 2002-2012 period are ranked in the top 10 of the most influential events on the stratospheric aerosol burden including: (1) The Kasatochi eruption (52.2° N; 175.5° W, Alaska) in 2008 which injected 1.5-2.5 Tg of SO_2 into the upper troposphere and lower stratosphere (UTLS) (Bourassa et al., 2010; Kravitz et al., 2010; Krotkov et al., 2010); (2) The Sarychev eruption in June 2009 (48.1°N; 153.2°E, the Kuril Island) which released 0.9 Tg of SO_2 into the UTLS (Clarisse et al., 2012; Kravitz et al., 2011; Jégou et al., 2013); (3) The Nabro eruption (13.4°N; 41.7°E, Eritrea) in June 2011 which emitted 1.3 Tg of SO_2 into the UTLS (Bourassa et al., 2012; Sawamura et al; 2012). In comparison, these recurrent moderate volcanic eruptions injected 10-20 times less SO_2 than the Pinatubo eruption (Solomon et al., 2011). These eruptions can also be used to

understand stratospheric dynamics as was done for the case of the Pinatubo eruption (Trepte et al., 1992).

Indeed, following a volcanic eruption, stratospheric aerosols can be used as a dynamical tracer (Bencherif et al., 2003; Fairlie et al., 2014). Based on satellite observations and a Lagrangian trajectory model, Fairlie et al. (2014) used the dispersion of the Nabro plume to study the dynamics of the Asian Monsoon Anticyclone. Hitchman et al. (1994) and SPARC (2006) suggested that the stratospheric aerosols distributions could be used to understand changes in the Brewer-Dobson Circulation. More recently, Ray et al. (2014) combined in situ balloon observations of SF_6, CO_2 with a numerical model to show that major explosive volcanic eruptions can induce large-scale changes in the stratospheric circulation via radiative perturbations, improving our understanding of stratospheric transport variability. Aerosols heating in the lower stratosphere induces a westerly wind anomaly, and enhanced tropical upwelling (Ray et al., 2014; Pitari et al., 2016a). Using the University of L'Aquila climate-chemistry model (ULAQ-CCM), Pitari et al. (2016a) analyzed the volcanic aerosols perturbation from the eruption of Mt. Pinatubo on the transport of long-lived species, N_2O and CH_4. They showed that the observed decline of long-lived greenhouse gases one year after the eruption is quantitatively consistent with enhanced stratosphere-troposphere exchange, due to a change in the Brewer–Dobson circulation. They also revealed that the volcanic aerosols radiative perturbation to stratospheric dynamics may be found by looking at the stratospheric age-of-air. According to Pitari et al (2016a), enhanced tropical upwelling tends to decrease the tropical age of air and the latitudinal age gradient after major volcanic eruptions. Although most studies discuss major tropical eruptions and their induced dynamical effects, we cannot exclude the possibility that extratropical eruptions in the last 15 years may also have had a significant role in lower stratospheric trends of key dynamical quantities (Kremser et al., 2016).

Previous works have also revealed that stratospheric aerosols can be used to study meridional air mass transport from the tropical stratospheric reservoir (Trepte and Hitchman, 1992; Randel et al., 1993; Chen et al., 1994; Grant et al., 1996, Vernier et al., 2009). Based on satellite observations, Trepte and Hitchman (1992) have shown that transport from the tropics to mid-latitudes is favored during westerly shear phases of the quasi-biennial oscillation (QBO) rather than during the easterly shear phases. More recently, by the use of satellite observations and climate models, Hommel et al. (2015) revealed that the vertical and latitudinal extent of the stratospheric aerosol layer (between 16 and 31 km) in the tropics is modulated by the QBO. Pitari et al. (2016b) analyzed the radiative perturbations in the stratosphere induced by the last five major volcanic eruptions after 1960 (i.e, Angung, St Helens, El Chicon, Nevado del Ruiz

and Pinatubo) using a climate model which included an aerosols microphysics module for aerosols formation and growth. They found an increase in stratospheric temperature associated with a significant impact on the tropical upwelling. The impact on stratospheric upwelling is found to be larger when the volcanically perturbed stratospheric aerosols are confined to the tropics, as tends to be the case for eruptions which are followed for several months with easterly shear of the QBO. They showed that the Nevado del Ruiz and Pinatubo eruptions occurred during years with dominant QBO easterly shear, which led to the confinement of the aerosols near the equator, with less poleward transport. This tropical confinement produced a larger latitudinal gradient of the perturbation heating rate and a stronger impact on the tropical upwelling (Pitari et al., 2016b). It is worth noting that the life cycle of an aerosol is affected by sedimentation. The fact that sulphuric particles grow larger following major eruptions (e.g. Russell et al., 1996; Bauman et al., 2003) means they can sediment appreciably during transport within the stratosphere, causing the plume transport to diverge from the expected isentropic trajectory. Even in moderate eruptions, where sulphuric particle growth may not be significant, the accommodation of sulphur on to ultra-fine ash particles has the potential to also change the fate of a proportion of the volcanic plume.

This paper reports on the Calbuco plume observations over Reunion Island (20.5°S; 55.5°E) and its transport in the southern tropics. The geometrical and optical properties of the Calbuco plume are inferred from the ground-based observations at Reunion Island in the framework of the MORGANE (Maïdo ObservatoRy Gas Aerosols NDACC Experiment) campaign. The aim of this study is to provide a description of the dynamical context which has favored the spread of the Calbuco plume in the Southern Hemisphere. The paper is organized as follows: Section 2 describes the observations and the model used for the investigation of the volcanic aerosol transport. A description of the long-range transport of the volcanic plume over the Indian Ocean is provided in Section 3; Section 4 gives a dynamical analysis of this case study; and the summary and the conclusions are given in Section 5.

2. Instrumentation and model description

2.1 Observations

2.1.1 Ground-based LiDAR

One part of the observations used in this study was performed during the MORGANE campaign which took place at the Maïdo observatory on Reunion Island in May 2015. The MORGANE ground-based observational systems combine LiDAR and balloon-borne payloads to study the

composition and the dynamics of the UTLS in the southern hemisphere. Among measurement data from four LiDAR systems operated during this campaign, we used data from the Differential Absorption Lidar (DIAL) system built for stratospheric ozone monitoring (Baray et al., 2013). It is also possible to retrieve aerosol profiles in the 15-38 km altitude range from these measurements. This instrument has been in operation at the Maïdo observatory since early 2013. The technical details and evaluation of its performance are given by Baray et al., (2013). A brief description of this DIAL system follows. It uses a frequency-tripled Nd:YAG laser, which provides a beam at 355 nm wavelength, with a repetition rate of 30 Hz and a XeCl excimer laser which emits radiation at 308 nm at 40 Hz. The optical receiver is a telescope composed of 4 parabolic mirrors where the backscattered signal is collected by 4 optical fibers located at the focal points. The current configuration of the DIAL LiDAR system mainly detects signals in the UV regions of the spectrum (308, 332, 355 and 387 nm). The LiDAR data set used in this study consists of daily records of backscattering signal obtained from the Maido facility between 1 November 2014 and 30 November 2016 (106 profiles). It should be noted that no measurements were recorded at Reunion Island from January to April 2016 because of technical problems. The daily measurements are nighttime and time-integrated over about 3 hours in average.

We used the methodology described by Sasano (1985) to obtain the extinction and backscatter coefficient from a Rayleigh-Mie LiDAR. This methodology is similar to the approach of Klett (1981) with the advantage of providing a numerical calculation of the extinction and backscatter coefficient. Temperature and pressure profiles are needed to retrieve optical properties from this approach. For this study temperature and pressure profiles obtained from a radiosondes launched from the airport of Gillot at 11h (UTC) are used**.** In order to obtain a complete temperature and pressure profiles range from the ground to mesosphere, we used the Arletty atmospheric model (Hauchecorne et al., 1998; Nair et al., 2012), based on European Centre for Medium Range Weather Forecast (ECMWF) data. The altitude of reference is determined for each profile. On average, the reference altitude is located between 30 and 40 km. Another parameters that we need to retrieve the optical properties is the ratio of backscatter and the extinction coefficient for aerosol, also called lidar ratio. For background stratospheric aerosol, the value found in the literature is near 60 (Trickl et al., 2013 ; Ridley et al., 2014; Sakai et al., 2016; Khaykin et al., 2017). This value is commonly used for volcanically quiescent conditions and periods of moderate eruptions (Sakai et al., 2016). The LiDAR ratio depends on the particle size distribution and the type of aerosol (Jäger and Deshler, 2002; Young and Vaughan, 2009).

Error in the LiDAR ratio could influence significantly the uncertainty on aerosols extinction and optical depth (Sakai et al., 2016; Khaykin et al., 2017). Moreover, it should be noted that new approaches to derive extinction from LiDAR, which also measure depolarization, have been developed and already applied to space-borne lidar such as CALIOP (Young and Vaughan, 2009).

2.1.2 Balloon-borne OPC.

In order to analyze the evolution of the concentration and the size of the observed aerosols over the Reunion Island site, many LOAC (Light Optical Aerosols Counter) systems were launched together with balloon-ozonesondes. A detailed description of the LOAC is given by Renard et al. (2016). In brief, LOAC is a lightweight Optical Particle Counter (OPC) of 1 kg which can fly under latex weather balloons. Through the measurements of the light scattered by particles at two specific angles (Lurton et al. 2014), the LOAC provides aerosols concentrations and particle size distributions for 19 size classes ranging from 0.2 µm to 50 µm in diameter every ten seconds with a vertical resolution of nearly 50 m depending on the ascent rate of the balloon. The number concentration range is from 0.6 to a few thousand particles per cm^3 (Vignelles, 2017). Uncertainties on number concentration during the ascent under meteorological balloon are mainly due to temperature variation effects on electronics (Renard et al., 2016, Vignelles, 2017). Uncertainties on number concentrations for size bins smaller than 1 µm is estimated to be ± 30 %. For larger size bins, uncertainties on number concentration are governed by Poisson statistics and estimated to be ± 20 % and ± 60 % at particle concentrations lower than 10^{-1} and 10^{-2} cm^{-3}, respectively.

2.1.3 CALIOP

The Cloud-Aerosols Lidar with Orthogonal Polarization (CALIOP) on board The Cloud-Aerosols Lidar and Infrared Pathfinder Satellite Observation (CALIPSO) was used to study the transport of the Calbuco plume. CALIPSO was launched to a Sun-synchronous polar orbit in 2006 (Winkler et al., 2009) with a repeat cycle of 16 days. CALIPSO is composed of an Infrared Imager Radiometer (IIR), a wide field visible camera and the CALIOP LiDAR. CALIOP is a two-wavelength polarization-sensitive LiDAR (532 and 1064 nm) which measures total attenuated backscatter vertical profiles with altitude-varying vertical (30-300 m) and horizontal (300-5000 m) resolution (Winker et al., 2009). The data used in this study are the total and perpendicular backscatter coefficient at 532 nm, available from the CALIOP level 1B V4.01 product. These data have been averaged every 1 degree in latitude for each orbit and grouped

into data files containing 16 days of measurements. From there, the scattering ratio and depolarization ratio at 532 nm have been calculated (Vernier et al., 2009). Through the use of this algorithm, the full zonal means of scattering ratio between 20°S and 20°N are obtained by averaging 7200 cells, leading to a precision of ± 1.6 % (Vernier et al., 2009). The ability of CALIOP to detect small volcanic plumes in the lower tropical stratosphere has been highlighted in previous studies (Thomason et al., 2007; Vernier et al., 2009, 2011).

2.1.4 IASI

The Infrared Atmospheric Sounding Interferometer (IASI) observations were used to quantify the amount of SO_2 emitted during the Calbuco eruption. IASI is a nadir view thermal infrared sounder on board the Meteorological Operational satellite (MetOp-A and MetOp-B). The IASI observations used in this study were realized from the MetOp-A platform which launched in October 2006. The IASI global spatial coverage and footprint of 12 km make it relevant for monitoring of the key atmospheric species, in particular for the volcanic SO_2 (Clarisse et al., 2008, 2012; Clerbaux et al., 2009). The amount and altitude of emitted SO_2 were obtained from the algorithms detailed in Clarisse et al. (2012) and Clarisse et al. (2014) respectively. For each IASI observation, the altitude was estimated first, after which the column was calculated using the altitude information as an input parameter.

2.1.5 OMPS

The Ozone Mapper and Profiler Suite (OMPS) Limb Profiler (LP) is also used in the present study to analyze the optical properties of the volcanic plume over the Reunion Island site. OMPS was launched in October 2011 on board the Suomi National Polar Partnership (NPP) spacecraft. The data used in this study are the daily extinction profiles at 675 nm. A detailed description of the aerosol extinction retrieval algorithm is given by Jaross et al. (2012) and Rault and Loughman (2013). Briefly, the aerosol extinction profiles are retrieved from the scattering solar radiation. The aerosols extinction are retrieved using spectral channels with weak gaseous absorption. Rodgers' maximum likelihood technique is used to retrieve the aerosol extinction profiles independently for each wavelength s (Taha et al., 2011). We used 2 years (From November 2014 to November 2016) of satellite overpasses above the LiDAR site, within a 5°x5° in latitude and longitude grid. OMPS data have already used to be very effective at detecting and characterizing major events, such as the Chelyabinsk bolide in February 2013 (Gorkavyi et al., 2013).

2.2 MIMOSA model

The Modèle Isentropique de transport Mésoéchelle de l'Ozone Stratosphérique par Advection (MIMOSA) model (Hauchecorne et al., 2002) is a Potential Vorticity (PV) advection model running on isentropic surfaces (surface of constant potential temperature). The advection scheme is semi-Lagrangian with a time step of 1 hour. The re-gridding onto the original orthonormal grid is performed every 6 hours. The model resolution is 0.5°x0.5°. The advection is driven by ECMWF meteorological analyses at a resolution of 0.5°x0.5°. In the case of the PV, its slow diabatic evolution is taken into account by relaxing the model PV towards the PV calculated from the ECMWF fields with a relaxation time of 10 days. Using this procedure, it is possible to run the model continuously and follow the evolution of PV filaments for several months. The accuracy of the model has been evaluated by Hauchecorne et al. (2002) and validated against airborne LiDAR ozone measurements using a correlation between PV and ozone, a quasi-conserved chemical tracer on timescales of a week or so within most of lower stratosphere (Heese et al., 2001; Jumelet et al., 2009). The MIMOSA model can also be used to determine the origin of air masses influencing a given site, similar to an isentropic Lagrangian trajectory model. The MIMOSA model is frequently used to detect the origin of air masses inducing laminae on ozone profiles (Hauchecorne et al., 2002; Godin et al., 2002; Portafaix et al., 2003).

2.3 DyBAL code

The Dynamical BArrier Location (DyBAL) code is an original software developed at the Laboratoire de l'Atmosphere et des Cyclones (LACy, France) to detect barriers to mixing in the subtropical stratosphere (Portafaix et al., 2003). The dynamical barriers are detected from the equivalent length of the tracer contour and the gradient of isentropic Ertel's potential vorticity (PV) in equivalent latitude coordinate as defined by Nakamura (1996). These two diagnostic tools are used by DyBAL to identify weak mixing and transport barriers. The position of the dynamical barrier is characterized by a local maximum of the PV gradient and a local minimum of the equivalent length (Nakamura, 1996). The DyBAL code is applied to the PV map obtained from the MIMOSA model runs. The ability of DyBAL to detect the position and the deformation of the dynamical barriers has been highlighted in previous studies (Bencherif et al., 2007; Morel et al., 2005; Portafaix et al., 2003).

3. Long-range transport and evolution of the Calbuco volcanic plume over the Indian Ocean

3.1 Plume formation and transport

3.1.1 SO_2 plume

After 43 years of inactivity, Calbuco erupted on 22 April 2015 and two intense explosive events were recorded during the same week. The evolution of the SO_2 total mass measured by IASI between 23 April 2015 and 31 May 2015 is reported in Figure 1. The SO_2 total mass is defined as the sum of SO_2 mass over the atmospheric column from midday to midnight over the southern hemisphere. As expected an increase of the SO_2 amounts was observed by IASI a few days following the Calbuco eruption. One day after the eruption the SO_2 total mass was 10 times higher than background levels. The SO_2 total mass increased quickly to its maximum value (0.41 Tg) on 25 April 2015 and slowly decreased to reach values close to the background values on 19 May 2015 (Fig. 1). The SO_2 e-folding time was estimated to be about 11 days that is in agreement with the time value reported for the 2009 Sarychev volcanic eruption (Jégou et al., 2013). The SO_2 total mass increased again on 28 May 2015 to reach a secondary maximum (0.13 Tg) on 30 May 2015. This new increase of the SO_2 total mass could be due to the Wolf eruption (Isabela Island, Galapagos) which occurred on 25 May 2015 (Xu et al., 2016). The maximum SO_2 total mass (0.41 Tg) emitted during the Calbuco eruption was about two times lower than the maximum value (0.9 Tg) emitted from the Sarychev eruption (0.9 Tg) in June 2009 (Jégou et al., 2013). It is also worth noting that the SO_2 mass injected during the Calbuco eruption is of the same order as for the Grimsvötn eruption in May 2011 (Clarisse et al., 2011). Figure 2 also depicts the maximum altitude of SO_2 over the period from 23 April 2015 to 31 May 2015. On average the maximum altitude of SO_2 is located in the lower stratosphere region around 17 km.

The SO_2 measurements integrated from midday to midnight obtained from IASI are also used to describe the transport of the volcanic plume over the southern hemisphere (Fig. 2). On 23 April 2015, a part of the Calbuco plume passed close to the Uruguay coast at an altitude of 17 km and then was transported by the general circulation. The plume reached Southern Africa and East side of Madagascar on 1 May 2015 at altitude of 17-18 km and was organized following a cyclonic rolling (Fig. 2b). On 6 May, the plume was mainly located over the Atlantic Ocean near the west coast of South Africa and partly over Namibia and South Africa. As expected, the SO_2 plume extent and amplitude began to diminish on 11 May 2015 by the oxidation of SO_2 to gaseous sulphuric acid which is further converted into H_2SO_4-H_2O liquid aerosol. The plume was embedded in a thin 15-17 km altitude atmospheric layer, extending from the Atlantic Ocean to the Indian Ocean passing over the Cape of Good Hope (Fig. 2d).

3.1.2 Spatial extent of the aerosol plume

The transport of the volcanic aerosols plume over the Southern Hemisphere can be followed by CALIOP observations at 532 nm. Figure 3 shows the CALIOP cross-section of the 532nm total attenuated backscatter (TAB) for the overpass over South America on 24 April. The TAB signals ranging from 1 10^{-3} to 5 10^{-3} km^{-1} sr^{-1} corresponding to weak values of brightness temperatures over the southern part of Brazil (34.22°S; 53.97°W) can be attributed to volcanic material injected up to the lower stratosphere by the Calbuco eruption. Figure 4 and 5 present the latitude-altitude cross sections of the scattering ratio observed by CALIOP for 16-day selected periods in 2015. The data displayed in Figure 4 and 5 correspond to the zonal mean averages of CALIOP scattering ratio during 16-day periods. The data are calculated within 1° latitudinal zonal bands and have about 9% error (Vernier et al., 2009). The scattering ratio (SR) values observed during the 16-30 April period (before the eruption) in the Southern hemisphere, particularly in the lower stratosphere, were in average at 1.05 (not shown). Between one and three weeks after the eruption (1-16 May period), CALIOP observations reveal that SR increased up to 1.12 in the southern lower stratosphere (Fig. 4a). The amplitude of the plume during the first weeks following the eruption was higher than the background aerosol levels at mid-latitudes but was still below the scattering ratio values observed in the tropics. The first weeks following the eruption correspond to the period when the SO_2 is still being converted into H_2SO_4-H_2O liquid aerosols (Fig. 1). The elevated backscatter in the tropics could be attributed to possible remnants of the Kelud (7.5°S; 112.2°E; erupted in February 2014) volcanic aerosol superimposed to the equatorial background aerosol layer (Kristiansen et al., 2015). About one month after the eruption (16-31 May period) the Calbuco plume was much more pronounced with scattering ratio values (ranging from 1.16 to 1.18) largely above values observed before the eruption from CALIOP and greater than aerosols amounts confined in the tropical reservoir (Fig. 4b). The second half of May (16-31 May) corresponds to the period when SO_2 has been oxidized to aerosol. The plume extended up to about 20 km in altitude and spread over a wide range of latitudes, nearly reaching 60°S and intruding into low latitudes near 5°S. About one month later (16-30 June), the plume top had moved upward by several hundred meters and the layer was thicker (Fig. 5a). The Southern Hemisphere between 10°S and polar latitudes was full of volcanic aerosols with scattering ratio values much higher than elsewhere in the whole stratosphere. About four months after the eruption (16-31 August) the volcanic aerosols layer was even thicker with scattering ratio remaining high (Fig. 5b). Figure 5b also

reveals a deepening of the volcanic aerosols layer and an enhancement of the equatorial backscatter in the Upper Troposphere.

In the 21-28 km altitude range, detrainment of aerosols from the equatorial reservoir depends upon the phase of the QBO and on the intensity of planetary wave activity (Trepte and Hitchman, 1992). Through the use of numerical model, Pitari et al (2016b) discussed on the impact of the QBO phase on the meridional transport of the aerosols plume to mid- and high latitudes. They revealed that the volcanic aerosols is confined to the tropics when the volcanic eruption occurred during the easterly shear of the QBO. When QBO easterlies descend in the tropics, propagation of planetary waves is inhibited from entering this region, thus limiting the extent to which these waves may detrain aerosol laterally from the tropical reservoir (Trepte et al., 1993). This corresponds to the situation in April-May, 2015 (Figure 4a, b). However, during the westerly phase of the QBO, mixing across the subtropics is favored, especially in winter (Trepte et al., 1993). The meridional spread in aerosols to southern midlatitudes shown above 21 km in Figure 5a and 5b is consistent with the phase reversal of the QBO from easterlies to westerlies observed from mid-2015.

3.2 Evolution of the aerosols plume over the Reunion site

3.2.1 Ground-based and satellite observations

Figure 6 depicts the evolution of the stratospheric AOD (sAOD) at 532 nm calculated between 17 and 30 km from the Reunion ground-based LiDAR and OMPS observations over Reunion Island from November 2014 to November 2016. The wavelength conversions to 532 nm were performed using the Angström exponents where detailed description of the methodology is given by Khaykin et al (2017). The Angström exponents for the 355-532 nm and 532-675 nm pairs were adopted from Jäger and Deshler (2002) and Khaykin et al (2017) set to -1.3 and -1.8 respectively. sAOD were calculated from LiDAR and OMPS observations at 532 nm using Angstrom exponent mentioned previously. As expected, an increase in the aerosol loading was observed over the Reunion site a few weeks after the Calbuco eruption. OMPS data show a doubling in the sAOD record in comparison with values observed at the end of 2014 and at the beginning of 2015 (Fig. 6). sAOD reached its maximum values (0.014 for OMPS) at the beginning of June 2015, decreased afterward to 0.01 on August 2015 and went back to pre-eruption values (0.004-0.006) in April 2016. The LiDAR record peaks at the same period, but sAOD values are 1.2 times weaker than those observed by OMPS during the June-December period. The LiDAR sAOD observations show less difference with values obtained prior to the

eruption (0.008). Discrepancies between OMPS and LiDAR were significantly reduced by April 2016, (cf. relative differences of 25% over the January-December 2015 period and 10% over the April-November 2016 period). From both datasets an aerosols e-folding of approximately 90 days can be derived, which is rather close to the value (~80 days) reported for the Sarychev eruption (Jégou et al., 2013).

Figure 7a illustrates the weekly-averaged extinction profiles at 532 nm derived from LiDAR measurements over Reunion Island. This figure reveals a sharp increase of the extinction between 18 and 19 km in May 2015 and reaching its maximum value (greater than 4 $x10^{-3}$ km^{-1}) in June. The vertical extent of the plume had increased significantly over the May-July period with a volcanic aerosols layer spanning from 18 to 21 km. At the beginning of June, the plume was structured in two layers with the first one centered at 18.5 km and the second one at 20 km (Fig.7a). We note also a brief decrease in the local extinction, ranging from 1.5 to 3 km^{-1}, around mid-May. The variability observed in the weekly-averaged extinction profiles and in the vertical extent of the aerosols signal over the May-July period reflects the presence of transient aerosol layers above Reunion Island and indicates that the plume is not homogeneously distributed at this stage. The altitude of the volcanic aerosols plume and the extinction values decreased from mid-August onwards. The plume is hence centered around 18 km in September, and extinction values in September are around two times less than those observed in June. This decrease of the extinction values is accompanied by a decrease of the altitude of the plume and could be due to the sedimentation processes (Fig. 7a). Hamil et al (1997) revealed that sedimentation can play a significant role in loss of stratospheric aerosols to the troposphere. Overall, the temporal evolution of the weekly-averaged extinction presents similar general features as the LiDAR observations, with maximum values in June and a subsequent gradual decrease of the aerosol signal. Nevertheless, in the OMPS data the plume is smeared out over a wider vertical range than in the lidar record (Fig. 7b). The vertical and horizontal structures of the plume are not reproduced in the OMPS data. In particular, the decrease in the plume altitude in mid-August is not observed by OMPS. More generally, extinction values observed by OMPS in the 15-17 km altitude range are higher than those observed by the LiDAR. The evolution of the scattering ratio at 532 nm obtained from the LiDAR and CALIOP space-borne observations during the April-December 2015 period over the Reunion Island site are presented on Figure 8. The scattering ratios from CALIOP have been averaged within $\pm 5^{\circ}$ in latitude and $\pm 50^{\circ}$ in longitude (extending from Africa to Australia) around Reunion Island (Fig. 8b). CALIOP observations confirm the presence of the volcanic aerosols plume over the Reunion

Island site at the beginning of May 2015 with maximum scattering ratio values (greater than 1.9) on mid-May 2015. Overall, the aerosols variability is smoother in CALIOP observations than in the LiDAR record, which shows more fluctuations in the altitude of the volcanic plume. In contrast to the LiDAR and OMPS observations, CALIOP data do not show an increase in the vertical extent of the plume and maximum scattering ratio values at the beginning of June 2015. According to CALIOP, the scattering ratio begins to decrease in mid-June followed by a slight decrease of the altitude of the plume from the end of July (Fig 8b). From July onwards, the CALIOP aerosol scattering ratios decrease gradually with similar values as observed by the LiDAR. The decrease of the aerosols scattering ratio is associated with a descent in the altitude of the plume, which could be due to sedimentation, and is consistent with the observations from OMPS.

The reasons for these discrepancies between ground-based and satellite observations may be multiple but effects due to different spatial samplings cannot be excluded. The difference in vertical resolution between ground-based LiDAR and satellites (OMPS, CALIOP) which could be one possible cause at the origin of discrepancies. The discrepancies between the satellites and ground-based LiDAR could be significant when the difference of vertical resolution is high between these devices. We note that the vertical resolution of OMPS is 10 times lower than the ground-based LiDAR with 1.5 km and 0.15 km respectively (Jaross et al., 2012). Thus, the structures of the plume look smoother than those obtained from the ground-based LiDAR. In the case of CALIOP where the vertical resolution is better (~ 3 times less to the ground-based LiDAR), the differences in the structure of the plume are less. Moreover, the discrepancies existing between results presented in this study could be also due to horizontal resolution or different measurement techniques. Unlike satellite experiments that allow global observations, a ground-based LiDAR system is able to derive aerosols characteristics at a specific location. OMPS views the Earth's limb looking backward along the orbit track of approximately 125 km with a horizontal resolution of 50 km. It is difficult for OMPS to detect with accuracy small amount of aerosol at a local point with these weak vertical and horizontal resolutions. It is for this reason that the structure of the plume observed since July is not in agreement with the ground-based LiDAR. As we will discuss more details in Section 4, the dynamical context can induce an inhomogeneity of the plume. As a consequence, this inhomogeneity of the plume could lead to incorrect identification of the volcanic aerosols by the satellites.

3.2.2 In-situ observations

Four LOAC OPCs were launched over the Reunion Island site on 26 November 2014, 19 May 2015, 19 August 2015, and 2 November 2016 respectively. sAOD 532 nm were calculated following Mie Theory from fits to the observed size distributions at each level. LOAC observations also reveal an increase by a factor of 2 in the sAOD on 19 May 2015 (1.35×10^{-2}). sAOD decreases to 8.4×10^{-3} on 19 August 2015 followed by a return to pre-eruption levels by November 2016 (Fig. 6). The overall evolution of sAOD derived from LOAC compares fairly well to OMPS and to lidar observations, accounting for error bars (Fig. 6). The 10-second sampling rate of the LOAC instrument and the ascent velocity of the balloon determine the vertical resolution. The difference observed between the daily LiDAR and the in-situ data may be due to the 1-minute averaging of the in-situ data, which tends to smooth structure attributed to the volcanic aerosols.

Figure 9 illustrates the number (dN/dln(D)) and volume (dV/dln(D)) concentrations obtained from the LOAC OPC observations over the Reunion Island site on 19 May 2015 at 1746 UTC. LOAC OPC observations reveal a size distribution with decreasing concentrations for particle sizes larger than 0.2 µm (Fig. 9). The value of 0.2 µm represents the lower bound of the LOAC size range, so the data may miss possible secondary modes for smaller particles (Wilson et al., 2008). Particle concentrations for sizes larger than 1 µm are too low to be properly detected by the LOAC OPC and undoubtedly indicate a coarse mode. However there is no clear evidence for a bimodal distribution, as observed during the first weeks after the eruption of Mt. Pinatubo, an intense second mode possibly consisting of volcanic ash (e.g. Russell et al., 1996). The shape of the size distribution obtained during the Calbuco event is similar to that obtained by Kravitz et al. (2011) for the Sarychev eruption. As suggested by Kravitz et al. (2011), we can also assume that the Calbuco eruption did not eject enough material to create a bimodal structure over Reunion Island.

The effective radius derived from the LOAC OPC on 19 May is 0.17 ± 0.02 µm indicating that the particles observed several weeks after the Calbuco eruption are quite small. Interestingly, Jégou et al. (2013) reported that the effective radius obtained during the Sarychev event ranged from 0.15 to 0.20 µm more than one month after the eruption, in agreement with the results of O'Neill et al. (2012). Therefore, both eruptions are comparable in terms of size distribution shape and effective radius. Russell et al. (1996) reported that in the month following the Pinatubo eruption the mean effective radius did not differ greatly from pre-eruption values (i.e. 0.17 ± 0.07 µm in their study), possibly because a large number of particles with sizes both smaller and larger than 0.17 µm were injected (the latter consisting most likely of volcanic ash).

The integrated number of particles obtained over the full 19 size classes from 0.2 to 50 µm in diameter is presented in Figure 10. A local aerosols concentration enhancement is detected in the lower stratosphere (16.8-19 km) over Reunion Island on 19 May 2015 at 1746 UTC. A maximum concentration of about 150 particles.cm^{-3} (total number of particles: 730 ± 130 particles (±1σ)) is observed by the aerosols counter for particle sizes larger than 0.2 µm. Few in situ observations are available in the tropical region such as Reunion Island to provide a reference state of the background aerosols content. In comparison to LOAC flight on 26 November 2014 at 1442 UTC (five months before the eruption), the aerosols number concentration observed on 19 May 2015 is ~20 times higher. Three months later, another LOAC OPC was launched over the Reunion Island site but the in situ profile only partially shows the volcanic aerosols layer because of a telemetry loss. The aerosols number concentration obtained on 19 August 2015 at 1300 UTC over Reunion Island may reveal a tendency to return to concentration values observed before the eruption (Fig. 10), with a number concentration of 40 particles per cm^3 in the lower stratosphere. This tendency is confirmed with the LOAC flight conducted on 2 November 2016 at 2030 UTC with a total number concentration close to 20 particles.cm^{-3} in the lower stratosphere (Fig. 10).

The residence time of the aerosols particles in the stratosphere depends on the balance between the growth processes and the removal processes which are likely to be controlled by the dynamical context. In the following section, we will discuss the influence of the dynamical activity on the variability of the volcanic aerosols over the Southern Hemisphere.

4. Dynamical modulation of the aerosol plume

4.1 Long-range transport

In order to analyze the isentropic transport, the high resolution MIMOSA model has been used to produce a continuous evolution of PV fields for the period from 1 April 2015 to 31 August 2015. Four advected PV maps, derived for the 400 K isentropic level from the MIMOSA model, together with dynamical barrier locations derived from the DyBaL code are superimposed in Figures 11 and 12. The localization of the volcanic aerosols plume obtained from OMPS observations at 400 K ± 5 K isentropic level is also superimposed (Fig. 11 and 12). On 24 April 2015, a significant wave activity is observed, leading to a fairly mixed surf zone in the 20°S-60°S latitude band (not shown). The Calbuco plume is situated inside the surf zone and the plume was mixed equatorward. On 27 April 2015, the subtropical and mid-latitude barrier are detected following the Nakamura's formalism (described in Section 2.3) around 15°S (red line,

Fig. 11) and 40°S (blue line) in latitude respectively, limiting the geographical extent of the plume (Fig. 11a). Figure 11a shows clearly that the air masses containing aerosols cannot move beyond the south of Brazil because of the presence of the subtropical barrier. On 01 May 2015, the air masses were confined between the two dynamical barriers located in average at 25°S (red line, Fig. 11b) and 40°S (blue line, Fig.11b) in latitude respectively. The air masses were advected eastward between South Africa and Madagascar following the wave shape of the barrier, consistent with the OMPS observations near South Africa (Fig. 11b). The subtropical barrier previously located at 25°S (red line, Fig.11b) moved northward crossing South Africa. The air masses containing aerosol previously situated in the south side of Madagascar were transported northward and eastward following the displacement of the barrier and reached the Reunion Island site.

On 19 May 2015 (Fig. 12a), the volcanic aerosol plume was confined between the two dynamical barriers and advected eastward. At this stage, the presence of the subtropical barrier and the polar vortex seems to constrain the Calbuco plume inducing its transport eastward. Between end of May and beginning of June, the subtropical barrier has dissipated while the edge of the polar vortex was around ~40°S (blue line, Fig. 12b). The OMPS observations reveal that the most part of the plume was located over the southern African and the Indian Ocean region in June (Fig. 12b). On the following months of July and August, the polar vortex is clearly identified at 60°S (blue line, Fig. 12b) which is a classical pattern for the austral winter.

This present study discuss only on the transport of the volcanic aerosols plume at 400 K isentropic level (isentropic level where the Calbuco plume is detected at Reunion). Figure 4 and 5 reveal that the meridional transport of the plume occurred between 12 and 20 km. In particular, Figure 5b reveals also the possibility to the Calbuco aerosols plume to penetrate the polar vortex at the end of August 2015. This assumption seems to be consistent to the works reported by Ivy et al. (2017) and Solomon et al. (2016). Based on SD-WACCM (Specified Dynamics-Whole Atmosphere Community Climate Model) model and balloon observations at Syowa (69°S; 34.58°E), Solomon et al. (2016) discussed on the impact of the Calbuco plume on the deepest Antarctic ozone depletion observed in October 2015. They reveal that the integrated additional Antarctic ozone column losses averaged over the polar cap are between 5 and 13 DU following the Calbuco eruption. Through the use of FR-WACCM (free-running Whole Atmosphere Community Climate Model), Ivy et al. (2017) shown that the forced response to the eruption of Calbuco was an increase in the size of the ozone hole by 4.5 10^6 km^2.

4.2 Removal processes

As discussed above, in the lower stratosphere distributions of the aerosols are modulated (or mostly driven) by isentropic transport. However, particle removal processes should be considered. As reported by Kremser et al (2016), aerosol in the vicinity of the tropopause can be transported into the troposphere by variety of mechanisms. Hamill et al. (1997) reported that stratosphere-troposphere exchange (STE) on isentropic surfaces due to Rossby wave activity can be considered a significant dynamical process for removal of stratospheric aerosols. Depending on the strength of the Brewer-Dobson circulation, stratospheric materials such as aerosols can be rapidly transported from the tropics to high latitudes (Dhomse et al., 2006, 2014). Based on semi-Lagrangian and analyzed winds from ECMWF, Chen et al. (1995) investigated the extratropical STE on isentropic surfaces that intersect the tropopause. Above 340 K they found that STE exhibits a strong annual cycle where very little STE takes place in the winter hemisphere, but significant STE occurs in the summer hemisphere, particularly in the northern summer. The weak STE in the winter hemisphere is mainly due to the barrier effect of the strong PV gradient at the tropopause (Chen et al., 1995). Through the use of 10 years of LiDAR observations at Pasadena (34°N, 118°W; California), Menzies and Tratt. (1995) found a clear link between the aerosol optical properties in UT-LS and the active extratropical STE processes occurring the winter and early spring. The calculated stratospheric mass extrusion rate is consistent with a 45-day lifetime of lower stratospheric aerosols during this part of the year, which implies that extratropical STE is a significant sink for stratospheric aerosols (Menzies and Tratt, 1995). Given the potential of a STE event to impact the stratospheric aerosols loading, we cannot exclude its contribution (even though small) on the stratospheric aerosols loading at Reunion Island.

Dhomse et al. (2014) using the CCM model (UM-UKCA) discussed the influence of STE events on the budget of the stratospheric aerosols. In particular, they suggested that a general overestimation of STE in global composition climate models could lead to overestimated removal of aerosols from stratosphere into the troposphere. Through the use of ULAQ-CCM model, Pitari et al (2016b) shown that the efficiency of STE depends on large-scale transport following the down-welling branch of the Brewer-Dobson circulation together with gravitational settling. The long-range transport of a volcanic plume is less likely to be isentropic, due to sedimentation of ash or other large particles (with any accommodated sulphur) within the plume. The modulation of the plume over Reunion Island could be caused by particle removal processes such sedimentation (considered as the primary loss mechanism

of stratospheric aerosol) or by dilution of the stratospheric plume (Hamill et al, 1997; Rasch et al., 2008). Sedimentation is an effective removal mechanism for particles that survive long enough in the stratosphere to grow to larger sizes (Hamill et al., 1997).

We note the potential role of removal processes on the initial dispersion of volcanic aerosols, in particular co-emitted ultrafine ash particles, but do not explore this effect here. Highlighting removal processes from Figures 7 and 8 is somewhat complicated by the transience in plume altitudes especially in the LiDAR local data. The potential role of removal processes on the evolution of the plume requires further investigation and will form the basis for a forthcoming study.

5. Summary and conclusion

The long-range transport of the volcanic aerosol produced following the Calbuco eruption has been examined. The analysis focuses on the dynamical context which led to the spread of the aerosol plume over Indian Ocean between April 2015 and November 2016. The transport of the volcanic aerosols to the Indian Ocean was investigated by combining satellite (CALIOP, IASI, OMPS), and ground-based experiments: Optical Particle Counter (LOAC) and LiDAR, in addition to numerical tools: the DyBal code and the high-resolution MIMOSA model.

The amount of SO_2 injected into the atmosphere during the Calbuco eruption has been quantified using IASI observations. SO_2 mass emitted by the Calbuco eruption was about two times lower than for the moderate Northern Hemisphere eruption of Sarychev in June 2009, but had a similar SO_2 e-folding time (Jégou et al., 2013; Kravitz et al., 2011). It is found from CALIOP observations that the Calbuco aerosol layer was observable in the lower stratosphere, between 18 and 21 km, and spread exclusively in the Southern Hemisphere. OMPS observations reveal that the Calbuco plume reached the Indian Ocean two weeks after the eruption. It is shown from ground-based observations deployed at Reunion Island that SAOD increased by a factor of ~2 by the beginning of May 2015 and decreased afterward, returning to pre-eruption values by November 2016. The aerosols e-folding time is estimated to be ~90 days, close to the ~80 days reported for the Sarychev eruption (Jégou et al., 2013). Though the various datasets agree in terms of aerosols signal intensity, we report significant differences for the plume height and its variability, possibly as a result of different observations geometries, resolutions and spatial scales inherent to each instrument.

In situ measurements by the LOAC OPC have pointed out the impact of the Calbuco eruption on the lower stratospheric aerosol content over the Reunion Island site. Aerosols number

concentrations were 20 times higher than values observed before and one year after the eruption. On May 2015, the volcanic aerosol was characterized by an effective radius of 0.16 ±0.02 µm and a unimodal lognormal size distribution above 250 nm diameter. These microphysical characteristics are in agreement with previous studies focusing on the Sarychev eruption (Kravitz et al., 2011; Jégou et al., 2013).

Through the use of the MIMOSA model and the DyBAL code, it was clearly identified that the eastward transport of the volcanic aerosols occurred mainly in form of planetary-scale tongues. In particular, the combination of MIMOSA and DyBal simulations revealed that the transport of the volcanic aerosol plume eastward was confined between subtropical barrier and mid-latitude (polar vortex) dynamical barriers, within which most of the zonal transport took place. Our results support the assumption that the processes explaining the structure of the plume over the southern hemisphere had mainly a dynamical origin. Thus, the fluctuation of the subtropical barrier induced transient aerosol layers above Reunion Island and an inhomogeneous distribution of the plume between May and July 2015. The present study also supports the hypothesis that the modulation of a volcanic plume results from a contribution of both dynamical and microphysical processes. Fully understanding the contribution of the microphysical processes to the evolution of the volcanic plume over the southern hemisphere requires further investigation. This will be examined in a forthcoming study.

Acknowledgements

This work is supported by the Labex « Étude des géofluides et des VOLatils–Terre, Atmosphère et Interfaces - Ressources et Environnement (VOLTAIRE) (ANR-10-LABX-100-01). This study is integrated and supported by the LEFE project SATORI (Stratospheric Aerosols in the Tropic Observed from Reunion Island). The authors thank the LPC2E and UMS balloon launching team for their technical collaboration. We would especially like to thank the staff of the team working on the lidar systems at the Maïdo observatory. Lieven Clarisse is a research associate with the Belgian FNRS-F.R.S. The authors thank also the CALIOP team and Jean-Paul Vernier for processing and providing data. OMPS observations were obtained from OMPS website (https://ozoneaq.gsfc.nasa.gov/).We are also grateful to the CCUR team for the use of the TITAN supercomputer. We thank also Duncan Fairlie for his contribution to improve the English of this paper.

References

Arfeuille, F., B. P. Luo, P. Heckendorn, D. Weisenstein, J. X. Sheng, E. Rozanov, M. Schraner, S. Brönnimann, L.W. Thomason, and T. Peter: Modeling the stratospheric warming following the Mt. Pinatubo eruption: uncertainties in aerosol extinctions, Atmos. Chem. Phys., 13, 11221–11234, 2013.

Baray, J. L., Courcoux, Y., Keckhut, P., Portafaix, T., Tulet, P., Cammas, J. P., ... & Desmet, F. (2013). Maïdo observatory: a new high-altitude station facility at Reunion Island (21° S, 55° E) for long-term atmospheric remote sensing and in situ measurements. *Atmospheric Measurement Techniques*, *6*(10), 2865-2877.

Bauman, J. J., Russell, P. B., Geller, M. A. and Hamill, P. : A stratospheric aerosol climatology from SAGE II and CLAES measurements: 2. Results and comparisons, 1984–1999. J. Geophys.Res. 108, 4383. (doi:10.1029/2002JD002993, 2003

Bekki, S : On the possible role of aircraft-generated soot in the middle latitude ozone depletion, *J. Geophys. Res., 102*, 10,751-10,758, 1997

Bencherif, H., Portafaix, T., Baray, J. L., Morel, B., Baldy, S., Leveau and J., Diab, R. : LIDAR observations of lower stratospheric aerosols over South Africa linked to large scale transport across the southern subtropical barrier. *Journal of atmospheric and solar-terrestrial physics*, *65*(6), 707-715, 2003

Bencherif, H., Amraoui, L. E., Semane, N., Massart, S., Charyulu, D. V., Hauchecorne, A., and Peuch, V. H., Examination of the 2002 major warming in the southern hemisphere using ground-based and Odin/SMR assimilated data: stratospheric ozone distributions and tropic/mid-latitude exchange. *Canadian Journal of Physics*, *85*(11), 1287-1300, 2007

Bluth, G. J. S., Doiron, S. D., Schnetzler, C. C., Krueger, A. J., and Walter, L. S.: Global tracking of the SO2 clouds from the June 1991 Mount Pinatubo eruptions, Geophys. Res. Lett., 19, 151–154, doi:10.1029/91GL02792, 1992.

Borrmann, S., Solomon, S., Dye, J. E., Baumgardner, D., Kelly, K.K., and Chan, K. R.: Heterogeneous reactions on stratospheric background aerosols, volcanic sulfuric acid droplets, and type I PSCs: The effects of temperature fluctuations and differences in particle phase, J. Geophys. Res., 102, 3639–3648, 1997.

Bourassa, A. E., D. A. Degenstein, B. J. Elash, and E. J. Llewellyn : Evolution of the stratospheric aerosol enhancement following the eruptions of Okmok and Kasatochi: Odin-OSIRIS measurements, J. Geophys.Res., 115, D00L03, doi:10.1029/2009JD013274, 2010

Bourassa, A. E., McLinden, C. A., Bathgate, A. F., Elash,B. J., and Degenstein, D. A.: Precision estimate for Odin-OSIRIS limb scatter retrievals, J. Geophys. Res., 117, D04303, doi:10.1029/2011JD016976, 2012

Canty, T., Mascioli, N. R., Smarte, M. D., & Salawitch, R. J. (2013). An empirical model of global climate-Part 1: A critical evaluation of volcanic cooling. *Atmospheric Chemistry and Physics*, *13*(8), 3997.

Carn, S., L. Clarisse, and A. J. Prata : Multi-decadal satellite measurements of global volcanic degassing, J. Volcanol. Geotherm. Res., 99-134, 2016

Chen, P., J. R. Holton, A. O'Neill, and R. Swinbank : Isentropic mass exchange between the Tropics and extratropics in the stratosphere. *J. Atmos. Sci.*, **51,** 3006–3018, 1994

Chen, P: Isentropic cross-tropopause mass exchange in the extratropics. *Journal of Geophysical Research: Atmospheres*, *100*(D8), 16661-16673, 1995

Clarisse, L., Coheur, P. F., Prata, A. J., Hurtmans, D., Razavi, A., Phulpin, T., Hadji-Lazaro, J., and Clerbaux, C.: Tracking and quantifying volcanic SO2 with IASI, the September 2007 eruption at Jebel at Tair, Atmos. Chem. Phys., 8, 7723-7734, doi:10.5194/acp-8-7723-2008, 2008.

Clarisse, L., Hurtmans, D., Clerbaux, C., Hadji-Lazaro, J., Ngadi,Y., and Coheur, P.-F.: Retrieval of sulphur dioxide from the infrared atmospheric sounding interferometer (IASI), Atmos. Meas. Tech., 5, 581–594, doi:10.5194/amt-5-581-2012, 2012.

Clarisse, L., Coheur, P. F., Theys, N., Hurtmans, D. and Clerbaux, C.: The 2011 Nabro eruption, a SO_2 plume height analysis using IASI measurements. *Atmospheric chemistry and physics*, *14*(6), 3095-3111, 2014

Clerbaux, C., Boynard, A., Clarisse, L., George, M., Hadji-Lazaro, J., Herbin, H. and Wespes, C. Monitoring of atmospheric composition using the thermal infrared IASI/MetOp sounder. *Atmospheric Chemistry and Physics*, *9*(16), 6041-6054, 2009

Dhomse, S., Weber, M., Wohltmann, I., Rex, M.,and Burrows, J. P.,. On the possible causes of recent increases in northern hemispheric total ozone from a statistical analysis of satellite data from 1979 to 2003. *Atmospheric Chemistry and Physics*, *6*(5), 1165-1180, 2006

Dhomse, S. S., Emmerson, K. M., Mann, G. W., Bellouin, N., Carslaw, K. S., Chipperfield, M. P. and Dalvi, M. , Aerosol microphysics simulations of the Mt.~ Pinatubo eruption with the UM-UKCA composition-climate model. *Atmospheric Chemistry and Physics*, *14*(20), 11221-11246, 2014

Fairlie, T. D., J. P. Vernier, M. Natarajan, and K. M. Bedka (2014), Dispersion of the Nabro volcanic plume and its relation to the Asian summer monsoon, Atmos. Chem. Phys., 14(13), 7045-7057, doi:10.5194/acp-14-7045-2014.

Froyd, K. D., D. M. Murphy, T. J. Sanford, D. S. Thomson, J. C. Wilson, L. Pfister, and L. Lait : Aerosol composition of the tropical upper troposphere, Atmos. Chem. Phys., 9, 4363-4385, 2009

Fussen, D., F. Vanhellemont and C. Bingen, Evidence of transport, sedimentation and coagulation mechanisms in the relaxation of post-volcanic stratospheric aerosols, *Ann. Geophys.*, *19*, 1157-1162, 2001

Godin, S., M. Marchand, and A. Hauchecorne, Influence of Artic polar ozone depletion on the lower stratosperic ozone amounts at Haute-Provence Observatory (44° N, 60° E), J. Geophys. Res, 107(20), 10.1029/2001JD000516, 107(D20), 2002

Gorkavyi, N., D. F. Rault, P. A. Newman, A. M. d. Silva, and A. E. Dudorov : New stratospheric dust belt due to the Chelyabinsk bolide, Geophys. Res. Lett., 40(17), 47284733, doi:10.1002/grl.50788, 2013

Grant, W. B., Browell, E. V., Fishman, J., Brackett, V. G., Veiga, R. E., Nganga, D., .Long, C. S. : Aerosol-associated changes in tropical stratospheric ozone following the eruption of Mount Pinatubo. *Journal of Geophysical Research: Atmospheres*, *99*(D4), 8197-8211, 1994

Grant, W. B., E. V. Browell, C. S. Long, L. L. Stowe, R. G.Grainger, and A. Lambert : Use of volcanic aerosols to study the tropical stratospheric reservoir. *J. Geophys. Res.*, **101,**3973–3988, 1996

Guo, S., Bluth, G. J., Rose, W. I., Watson, I. M. and Prata, A. J : Re-evaluation of SO2 release of the 15 June 1991 Pinatubo eruption using ultraviolet and infrared satellite sensors. *Geochemistry, Geophysics, Geosystems*, *5*(4), 2004

Hamill, P., Jensen, E. J., Russell, P. B., and Bauman, J.J.: The life cycle of stratospheric aerosol particles, B.Am. Meteorol. Soc., 78, 1395–1410, doi:10.1175/1520-0477(1997)078, 2.0.CO;2, 1997.

Hauchecorne, A.: Ether, Service Arletty, Atmospheric Model Description, ETH-ACR-AR-DM-001, 22 p., 1998.

Hauchecorne, A., Godin, S., Marchand, M., Heese, B., and Souprayen, C. Quantification of the transport of chemical constituents from the polar vortex to midlatitudes in the lower stratosphere using the high-resolution advection model MIMOSA and effective diffusivity. *Journal of Geophysical Research: Atmospheres*, *107*(D20), 2002

Heese, B., Godin, S and Hauchecorne, A : Airborne lidar measurements of ozone filaments during METRO–A validation of PV advection model MIMOSA. *J. Geophys. Res*, *106*, 20-011, 2001

Hermann, M., J. Heintzenberg, A. Wiedensohler, A. Zahn, G. Heinrich, and C. A. M. Brenninkmeijer, Meridional distributions of aerosol particle number concentrations in the upper troposphere and lower stratosphere obtained by Civil Aircraft for Regular Investigation of the Atmosphere Based on an Instrument Container (CARIBIC) flights, J. Geophys. Res., 108(D3), 4114, doi:10.1029/2001JD001077, 2003.

Hitchman, M. H., M. McKay and C. R. Trepte (1994), A climatology of stratospheric aerosol, *J. Geophys. Res.*, *99*, 20,689-20,700.

Hofmann, D., Barnes, J., O'Neill, M., Trudeau, M., and Neely, R.:Increase in background stratospheric aerosol observed with lidar at Mauna Loa Observatory and Boulder, Colorado, Geophys.Res. Lett., 36, L15808, doi:10.1029/2009GL039008, 2009.

Hommel, R., Timmreck, C., Giorgetta, M. A. and Graf, H. F. (2015). Quasi-biennial oscillation of the tropical stratospheric aerosol layer. *Atmospheric Chemistry and Physics*, *15*(10), 5557, 2015

Ivy, D. J., S. Solomon, D. Kinnison, M. J. Mills, A. Schmidt, and R. R. Neely III : The influence of the Calbuco eruption on the 2015 Antarctic ozone hole in a fully coupled chemistry-climate model, Geophys. Res.Lett., 44, 2556–2561, doi:10.1002/2016GL071925, 2017

Jäger, H., and T. Deshler, Lidar backscatter to extinction, mass and area conversions for stratospheric aerosols based on midlatitude balloonborne size distribution measurements,Geophys. Res. Lett., 29(19), 1929, doi:10.1029/2002GL015609, 2002.

Jaross, G., Chen, G., Kowitt, M., Warmer, J;, Xu, P., Kelly, T. and Flittner, D : Suomi NPP OMPS Limb Profiler initial sensor performance assessment. In SPIE asia-Pacific Remote Sensing (pp. 852805-852805), International Society for Optics and Photonics, 2012

Jumelet, J., S. Bekki, P. Seifert, N. Montoux, J.-P. Vernier, and J. Pelon (2009), Microphysical modeling of a midlatitude "polar stratospheric cloud" event: Comparisons against multiwavelength ground-based and spaceborne lidar data, J. Geophys. Res., 114, D00H03, doi:10.1029/2009JD011776.

Jégou, F., Berthet, G., Brogniez, C., Renard, J. B., François, P., Haywood, J. M. and Godin-Beekmann, S. (2013). Stratospheric aerosols from the Sarychev volcano eruption in the 2009 Arctic summer. *Atmospheric Chemistry and Physics*, *13*(13), 6533-6552.

Junge, C. E., Chagnon, C. W. and Manson, J. E. (1961). Stratospheric aerosols. *Journal of Meteorology*, *18*(1), 81-108.

Kinnison, D. E., K. E. Grant, P. S. Connell, D. A. Rotman, *and* D. J. Wuebbles *(*1994*)*, The chemical and radiative effects of the Mount Pinatubo eruption, J. Geophys. Res., 99*(*D12*)*, 25705–25731, *doi:*10.1029/94JD02318.

Klett, J. D : Stable analytical inversion solution for processing lidar returns, Appl. Opt., 20, 211 – 220, 1981

Kravitz, B., Robock, A., and Bourassa, A.: Negligible climatic effects from the 2008 Okmok and Kasatochi volcanic eruptions,J. Geophys. Res., 115, D00L05, oi:10.1029/2009JD013525, 2010.

Kravitz, B., Robock, A., Bourassa, A., Deshler, T., Wu, D., Mattis, I., Finger, F., Hoffmann, A., Ritter, C., Bitar, L., Duck, T. J.,and Barnes, J. E.: Simulation and observations of stratospheric aerosols from the 2009 Sarychev volcanic eruption, J. Geophys.Res., 116, D18211, doi:10.1029/2010JD015501, 2011.

Kremser, S., Thomason, L. W., Hobe, M., *et al.* Stratospheric aerosol—Observations, processes, and impact on climate. *Reviews of Geophysics*, vol. 54, no 2, p. 278-335, 2016

Kristiansen, N. I., A. J. Prata, A. Stohl,and S. A. Carn : Stratospheric volcanic ash emissions from the 13 February 2014 Kelut eruption, *Geophys. Res. Lett.*, *42*,588–596, doi:10.1002/2014GL062307, 2015

Krotkov, N. A., M. R. Schoeberl, G. A. Morris, S. Carn, and K. Yang : Dispersion and lifetime of the SO2 cloud from the August 2008 Kasatochi eruption, J. Geophys. Res., 115, doi:10.1029/2010jd013984, 2010

Labitzke, K. and McCormick, M.: Stratospheric temperature increases due to Pinatubo aerosols, Geophys. Res. Lett., 19, 207–210, 1992.

Lurton, T., Renard, J.-B., Vignelles, D., Jeannot, M., Akiki, R., Mineau, J.-L. and Tonnelier, T.: Light scattering at small angles by atmospheric irregular particles: modelling and laboratory measurements, Atmos., Meas. Tech., 7, 931-939, 2014.

McCormick, M. P., Thomason, L. W., and Trepte, C. R.: Atmospheric effects of the Mt Pinatubo eruption, Nature, 373, 399–404, 1995.

Menzies, R. T and Tratt, D. M.: Evidence of seasonally dependent stratosphere-troposphere exchange and purging of lower stratospheric aerosol from a multiyear lidar data set. *Journal of Geophysical Research: Atmospheres*, *100*(D2), 3139-3148, 1995

Morel, B., Bencherif, H., Keckhut, P., Portafaix, T., Hauchecorne, A., and Baldy, S., Fine-scale study of a thick stratospheric ozone lamina at the edge of the southern subtropical barrier: 2. Numerical simulations with coupled dynamics models. *Journal of Geophysical Research: Atmospheres*, *110*(D17), 2005

Mossop, S. C : Stratospheric particles at 20 km altitude, Geochemica et Cosmochimica Acta, ol. 29, pp. 201—207, 1965

Murphy, D. M., Thomson, D. S and Mahoney, M. J : In situ measurements of organics, meteoritic material, mercury, and other elements in aerosols at 5 to 19 kilometers. *Science*, *282*(5394), 1664-1669, 1998

Nair, P. J., Godin-Beekmann, S., Froidevaux, L., Flynn, L. E., Zawodny, J. M., Iii, J. R. andLeblanc, T : Relative drifts and stability of satellite and ground-based stratospheric ozone profiles at NDACC lidar stations. *Atmospheric Measurement Techniques*, *5*(6063), 1301-1318, 2012

Nakamura, N., Two-dimensional mixing, edge formation, and permeability diagnosed in an area coordinate. *Journal of the atmospheric sciences*, *53*(11), 1524-1537, 1996

Neely, R. R., P. Yu, K. H. Rosenlof, O. B. Toon, J. S. Daniel, S. Solomon, and H. L. Miller (2014), The contribution of anthropogenic SO2emissions to the Asian tropopause aerosol layer, J. Geophys. Res., 119(3), 1571-1579, doi:10.1002/2013JD020578.

O'Neill, N. T., Perro, C., Saha, A., Lesins, G., Duck, T. J., Eloranta, E. W and Bourassa, A : Properties of Sarychev sulphate aerosols over the Arctic. *Journal of Geophysical Research: Atmospheres*, *117*(D4), 2012

Pitari, G., Cionni, I., Di Genova, G., Visioni, D., Gandolfi, I., & Mancini, E : Impact of stratospheric volcanic aerosols on age-of-air and transport of long-lived species. *Atmosphere*, *7*(11), 149, 2016a

Pitari, G., Di Genova, G., Mancini, E., Visioni, D., Gandolfi, I., & Cionni, I : Stratospheric aerosols from major volcanic eruptions: a composition-climate model study of the aerosol cloud dispersal and e-folding time. *Atmosphere*, *7*(6), 75, 2016b

Portafaix, T., Morel, B., Bencherif, H., Baldy, S., Godin-Beekmann, S., and Hauchecorne, A.. Fine-scale study of a thick stratospheric ozone lamina at the edge of the southern subtropical barrier. *Journal of Geophysical Research: Atmospheres*, *108*(D6), 2003

Pueschel, R. F., Snetsinger, K. G., Russell, P. B., Kinne, S. A., & Livingston, J. M : The effects of the 1991 Pinatubo volcanic eruption on the optical and physical properties of stratospheric aerosols. *Proceedings of IRS92: Current Problems in Atmospheric Radiation*, 183-186, 1992

Rasch, P. J., Tilmes, S., Turco, R. P., Robock, A., Oman, L., Chen, C. C. J. and Garcia, R. R., An overview of geoengineering of climate using stratospheric sulphate aerosols. *Philosophical Transactions of the Royal Society of London A: Mathematical, Physical and Engineering Sciences*, *366*(1882), 4007-4037, 2008

Randel, W. J., Gille, J. C., Roche, A. E., Kumer, J. B., Mergenthaler, J. L., Waters, J. W. and Lahoz, W. A. (1993). Stratospheric transport from the tropics to middle latitudes by planetary-wave mixing. *Nature*, *365*(6446), 533-535.

Rault, D.F and Loughmann,R.P : The OMPS Limb Profiler environmental data record algorithm theoretical basis document and expected performance, IEEE Transactions on Geoscience and Remote Sensing, 51(5), 2505-2527, 2013

Renard, J.B., Dulac, F., Berthet, G., Lurton, T., Vignelles, D., Jégou, F., Tonnelier, T., Thaury, C., Jeannot, M., Couté, B., Akiki, R., Verdier, N., Mallet, M., Gensdarmes, F., Charpentier, P., Duverger, V., Dupont, J.V., Mesmin, S., Elias, T., Crenn, V., Sciare, J., Giacomoni, J., Gobbi, M., Hamonou, E., Olafsson, H., Dagsson-Waldhauserova, P., Camy-Peyret, C., Mazel, C., Décamps, T., Piringer, M., Surcin, J., and Daugeron, D.: LOAC: a small aerosol optical counter/sizer for ground-based and balloon measurements of the size distribution and nature of

atmospheric particles – Part 1: Principle of measurements and intercomparison campaigns, *Atmos. Meas. Tech.*, 9, 1721–1742, doi:10.5194/amt-9-1721-2016, 2016.

Ridley, D. A., et al. : Total volcanic stratospheric aerosol optical depths and implications for global climate change, Geophys. Res. Lett., 41(22), 7763-7769, doi:10.1002/2014GL061541, 2014

Russell, P. B., Livingston, J. M., Pueschel, R. F., Bauman, J. J., Pollack, J. B., Brooks, S. L. and Dutton, E. G. (1996). Global to microscale evolution of the Pinatubo volcanic aerosol derived from diverse measurements and analyses. *Journal of Geophysical Research: Atmospheres*, *101*(D13), 18745-18763.

Sasano, Y., Browell, E. V. and Ismail, S : Error caused by using a constant extinction/backscattering ratio in the lidar solution. *Applied Optics*, *24*(22), 3929-3932, 1985

Sawamura, P., Vernier, J. P., Barnes, J. E., Berkoff, T. A., Welton, E. J., Alados-Arboledas, L. and Lange, D. (2012). Stratospheric AOD after the 2011 eruption of Nabro volcano measured by lidars over the Northern Hemisphere. *Environmental Research Letters*, *7*(3), 034013.

Siddaway, J. M., and S. V. Petelina (2010), Transport and evolution of the 2009 Australian Black Saturday bushfire smoke in the lower stratosphere observed by OSIRIS on Odin, J. Geophys. Res., 116, doi:10.1029/2010JD015162.

Solomon, S., Portmann, R. W., Garcia, R. R., Thomason, L. W.,Poole, L. R., and McCormick, M. P.: The role of aerosol variations in anthropogenic ozone depletion at northern midlatitudes, J. Geophys. Res.-Atmos., 101, 6713–6727, 1996.

Solomon, S., Stratospheric ozone depletion: A review of concepts and history, Rev. Geophys., 37, 275–316, doi:10.1029/1999RG900008, 1999

Solomon, S., Daniel, J. S., Neely III, R. R., Vernier, J.-P., Dutton, E. G., and Thomason, L. W.: The persistently variable "Background"stratospheric aerosol layer and global climate change,Science 333, 866, doi:10.1126/science.1206027, 2011.

SPARC 2006 Assessment of stratospheric aerosol properties (ASAP). Technical report WCRP-124/WMO/TD-No. 1295/SPARC report no. 4, SPARC, Toronto, Ontario, CA, pp. 322.

Solomon, S., D. J. Ivy, D. Kinnison, M. J. Mills, R. R. Neely III, and A. Schmidt, Emergence of healing in the Antarctic ozone layer, Science, 252(6296), 269–274, doi:10.1126/science.aae0061, 2016

Stenchikov, G. L., Kirchner, I., Robock, A., Graf, H. F., Antuna, J. C., Grainger, R. G., Lambert, A. and Thomason, L. 1998 Radiative forcing from the 1991 Mount Pinatubo volcanic eruption conditions. J. Geophys. Res. 103, 13 837–13 857. (doi:10.1029/98JD00693)

Stenchikov, G., A. Robock, V. Ramaswamy, M. D. Schwarzkopf, K. Hamilton, *and* S. Ramachandran, Arctic Oscillation response to the 1991 Mount Pinatubo eruption: Effects of volcanic aerosols and ozone depletion, J. Geophys. Res., 107*(*D24*), 4803, doi:*10.1029/2002JD002090, 2002.

Schuster, G. L., O. Dubovik, and B. N. Holben : Angstrom exponent and bimodal aerosol size distributions, J. Geophys. Res., 111, D07207, doi:10.1029/2005JD006328, 2006

Taha, G., Rault, D. F., Loughman, R. P., Bourassa, A. E., & Savigny, C. V. (2011). SCIAMACHY stratospheric aerosol extinction profile retrieval using the OMPS/LP algorithm. *Atmospheric Measurement Techniques*, *4*(3), 547-556.

Thomason, L. W., Pitts, M. C., & Winker, D. M. (2007). CALIPSO observations of stratospheric aerosols: a preliminary assessment. *Atmospheric Chemistry and Physics*, *7*(20), 5283-5290.

Thomason, L. W., S. P. Burton, B.-P. Luo and T. Peter , SAGE II measurements of stratospheric aerosol properties at non-volcanic levels, *Atmos.* Chem. *Phys.*, *8*, 983-995, 2008

Trepte, C. R., and Hitchman, M. H.: Tropical stratospheric circulation deduced from satellite aerosol data, Nature, Vol. 355, 626-628, 1992.

Trepte, C. R., Veiga, R. E., and McCormick, M. P. : The poleward dispersal of Mount Pinatubo volcanic aerosol, J. Geophys. Res., vol. 98, No. D10, 18,563-18,573, 1993.

Trickl, T., Giehl, H., Jäger, H. and Vogelmann, H : 35 yr of stratospheric aerosol measurements at Garmisch-Partenkirchen: from Fuego to Eyjafjallajökull, and beyond. *Atmospheric Chemistry and Physics*, *13*(10), 5205-5225, 2013

Vernier, J. P., Pommereau, J. P., Garnier, A., Pelon, J., Larsen, N., Nielsen, J., and McDermid, I. S., Tropical stratospheric aerosol layer from CALIPSO lidar observations. *Journal of Geophysical Research: Atmospheres*, *114*(D4), 2009

Vernier, J.-P., Thomason, L. W., Pommereau, J.-P., Bourassa, A.,Pelon, J., Garnier, A., Hauchecorne, A., Blanot, L., Trepte,C., Degenstein, D., and Vargas, F.: Major influence of tropical volcanic eruptions on the stratospheric aerosol layer during the last decade, Geophys. Res. Lett., 38, L12807,doi:10.1029/2011GL047563, 2011.

Winker, D., Vaughan, M., Omar, A., Hu, Y., Powell, K., Liu, Z., Hunt, Wand Young, S : Overview of the calipso mission and caliop data processing algorithms, *J. Atmos.*1139 *Oceanic Technol.*, *26*, 2310–2323, 2009

Vignelles, D. : Caractérisation des performances du nouveau mini compteur de particule LOAC embarqué sous ballon météorologique : application à l'étude de la variabilité spatiale et temporelle des aérosols de la haute troposphère et de la stratosphère - PhD Thesis, Univ. Orléans, 2017

Weigel, R., Hermann, M., Curtius, J., Voigt, C., Walter, S., Böttger, T and Borrmann, S : Experimental characterization of the COndensation PArticle counting System for high altitude aircraft-borne application. *Atmospheric Measurement Techniques*, *2*, 243-258, 2009

Wunderlich, F. and Mitchell, D. M : Revisiting the observed surface climate response to large volcanic eruptions. *Atmospheric Chemistry and Physics*, *17*(1), 485-499, 2017

Xu, W., Jónsson, S., Ruch, J. and Aoki, Y : The 2015 Wolf volcano (Galápagos) eruption studied using Sentinel-1 and ALOS-2 data. *Geophysical Research Letters*, *43*(18), 9573-9580, 2016

Young,R ., H. Houben, and O. Toon, Radiatively forced dispersion of the Mt. Pinatubo volcanic cloud and induced temperature perturbation in the stratosphere during the first few months following the eruption, Geophys Res. Lett.,2 1,369-372, 1994.

Zuev, V. V., Burlakov, V. D., Nevzorov, A. V., Pravdin, V. L., Savelieva, E. S. and Gerasimov, V. V : 30-year lidar observations of the stratospheric aerosol layer state over Tomsk (Western Siberia, Russia). *Atmospheric Chemistry and Physics*, *17*(4), 3067-3081, 2017

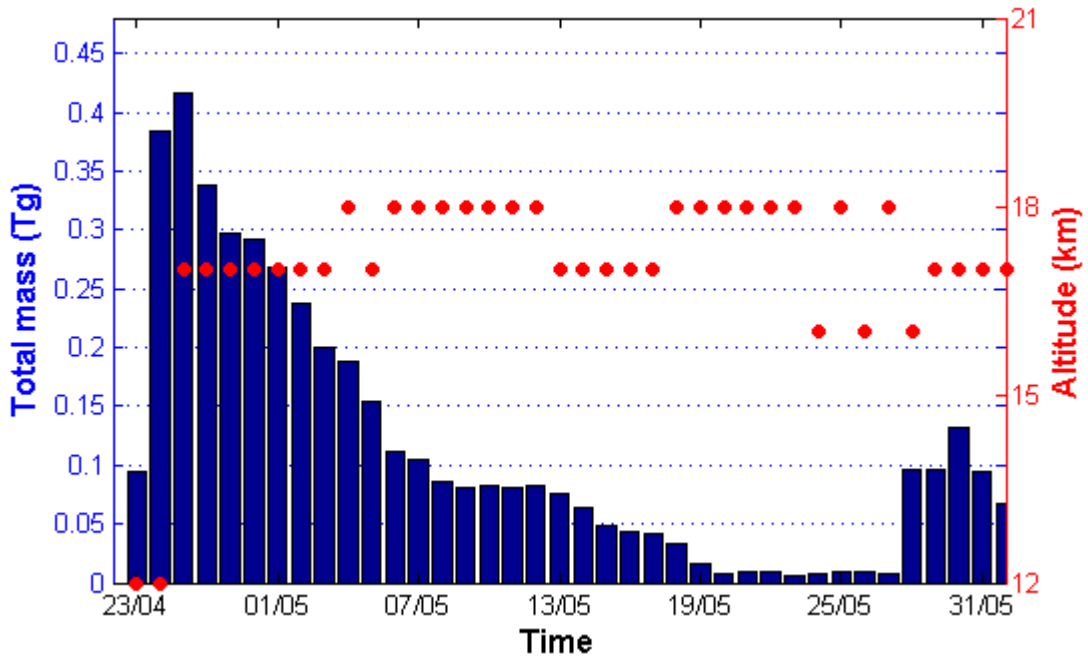

Figure 1 : Evolution of the SO_2 total column mass (in blue) and the altitude of the maximum SO_2 mass (red dots) obtained from IASI from 23 April 2015 to 31 May 2015 over the southern hemisphere. The altitude of the maximum SO_2 mass was obtained from the algorithms detailed in Clarisse et al. (2014).

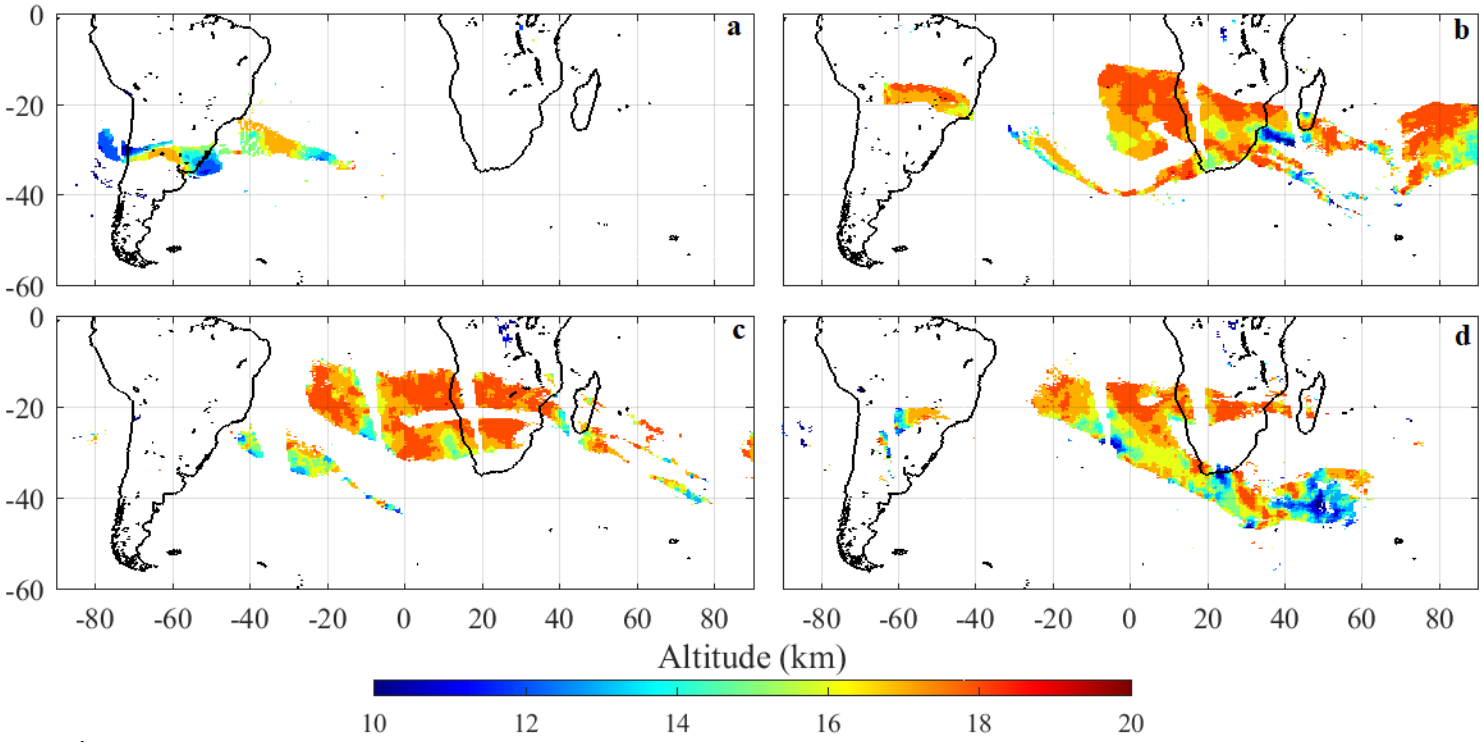

Figure 2 : Injection Altitude (km) and transport of SO_2 obtained from IASI observations during (a) 24/04, (b) 01/05, (c) 06/05 and (d) 11/05

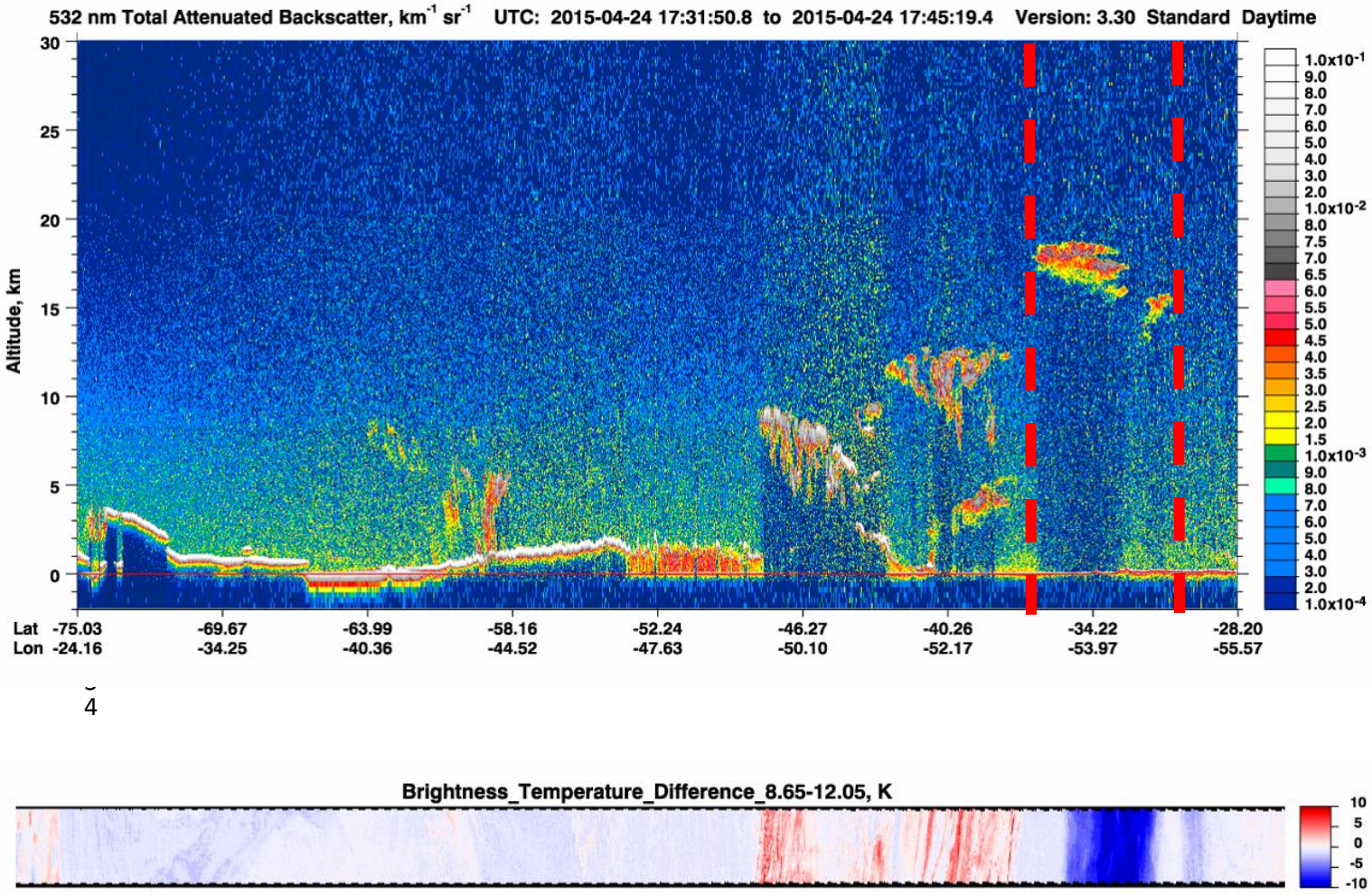

Figure 3 : CALIOP cross-section of 532 nm attenuated backscatter and Brightness temperature difference for the overpass at 1730-1745 on 24 April 2015 over South America from 28°S to 75°S latitude range. The two red dash lines delimited the geographical region where the Calbuco plume is observed by CALIOP on 24 April 2015.

a)

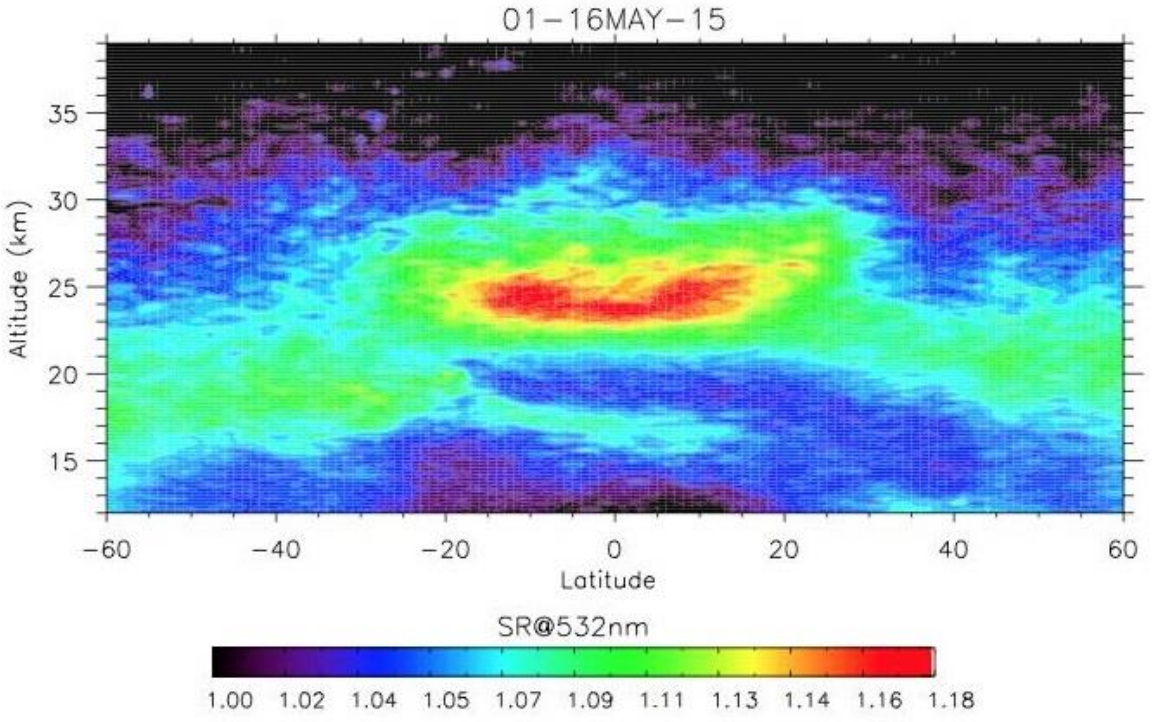

b)

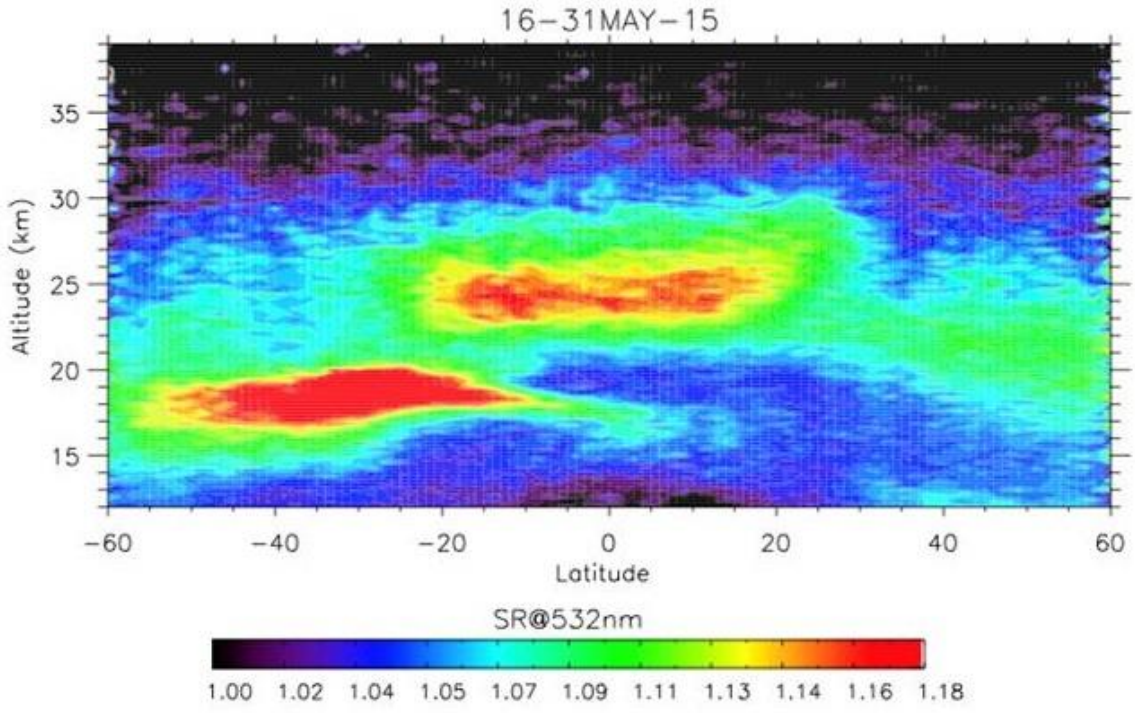

Figure 4 : Half monthly mean of the zonal scattering ratio at 532 nm in (a) 1-15 May (1-2 weeks after eruption), (b) 16-31 May (3-4 weeks after eruption).

a)

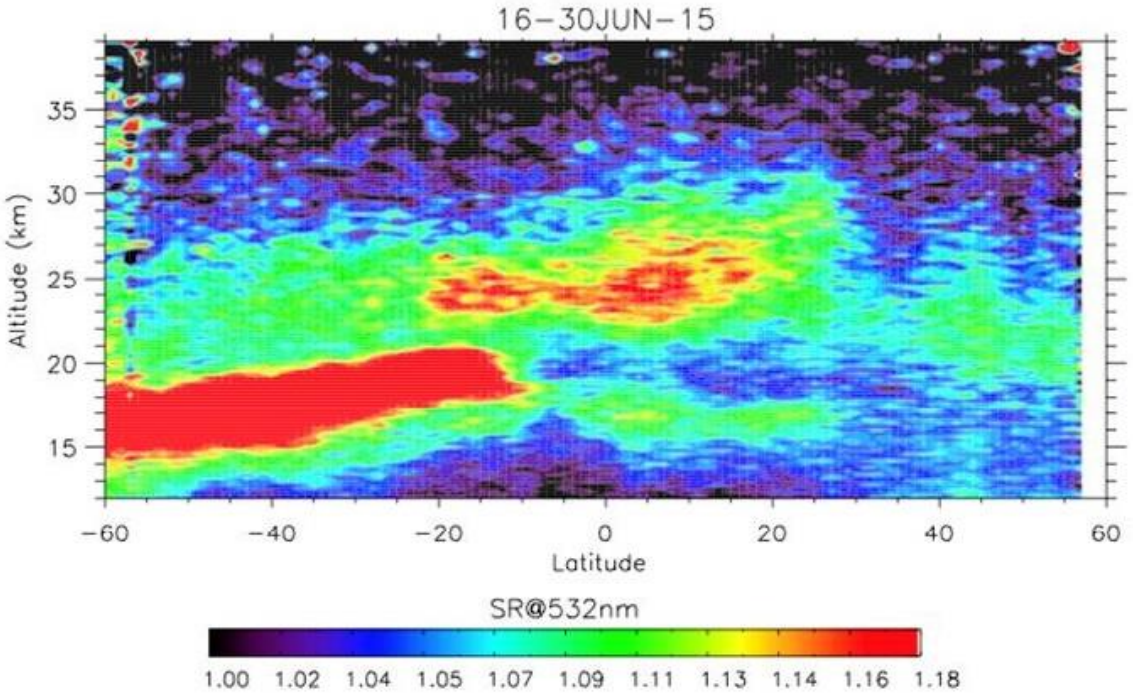

b)

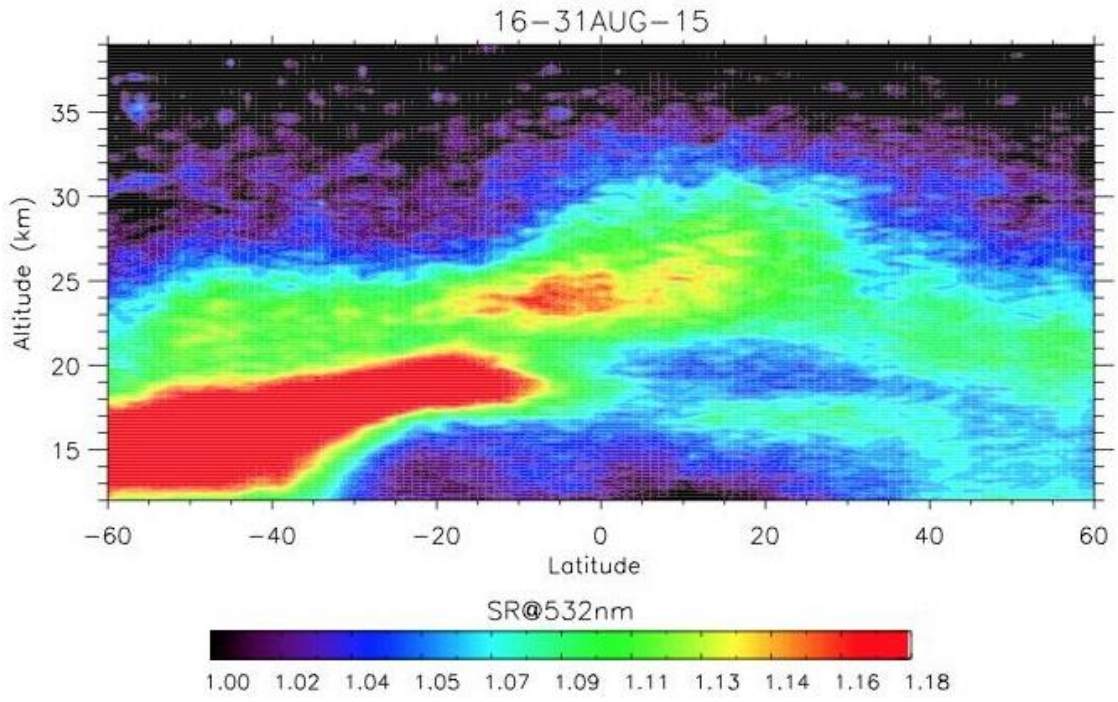

Figure 5 : Half monthly mean of the zonal scattering ratio at 532 nm in (a) 16-30 June (2 months after eruption) and (b) 16-31 August (4 months after eruption).

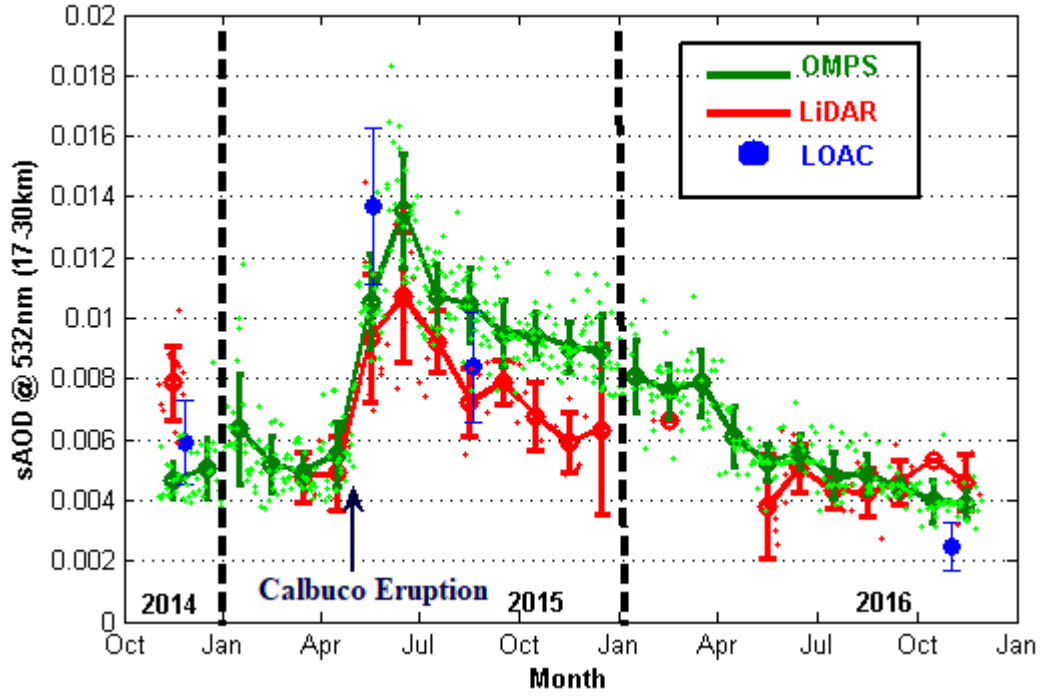

Figure 6 : Evolution of sAOD calculated between 17 and 30 km at 532 nm from LiDAR (red), LOAC OPC (blue) and OMPS (green) observations between November 2014 to November 2016 over the Reunion site. The small dots represent the daily sAOD and the large dots represent the monthly averaged sAOD obtained from OMPS and LiDAR observation. The large blue dots represent the sAOD calculated from LOAC OPC observations over Reunion during the 26 November 2014, the 19 May 2015, the 19 August 2015 and the 2 November 2016. The error bars associated to LiDAR and OMPS observations represent the standard deviation. The error bars associated to LOAC OPC represent the uncertainties values. The date of the Calbuco eruption is indicated by a blue arrow.

a)

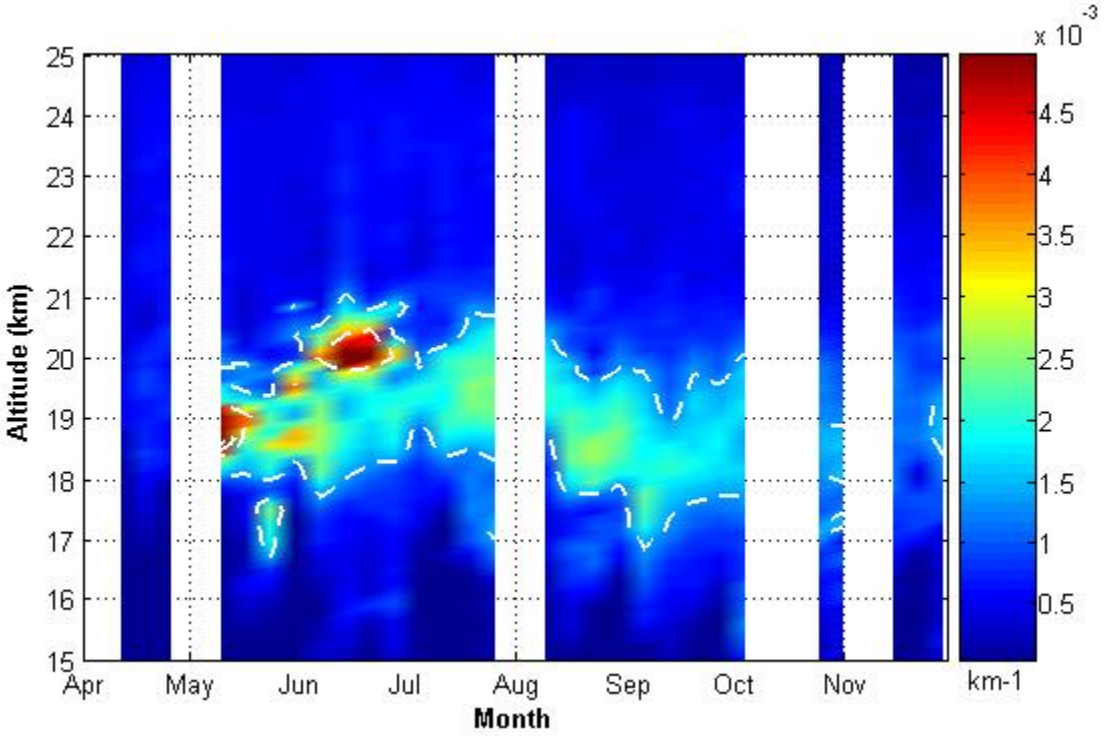

b)

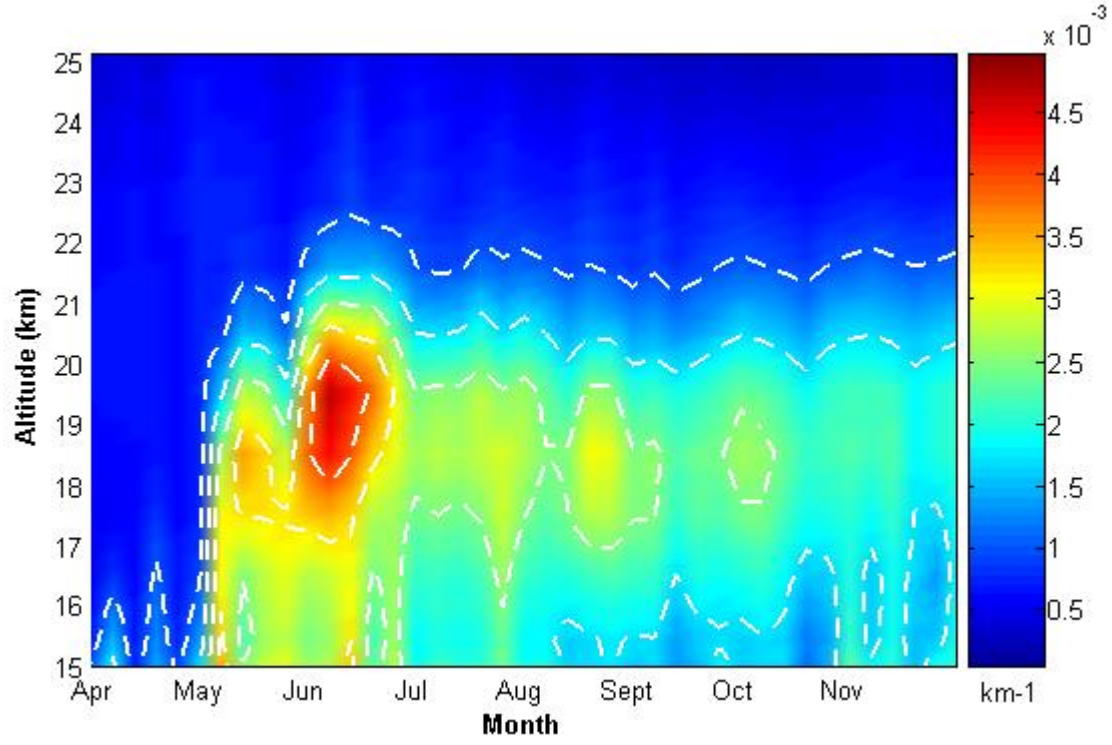

Figure 7 : Time series of weekly-averaged profiles of extinction at 532 nm obtained from (a) ground-based LiDAR and (b) OMPS observations over Reunion between April 2015 and December 2015.

a)

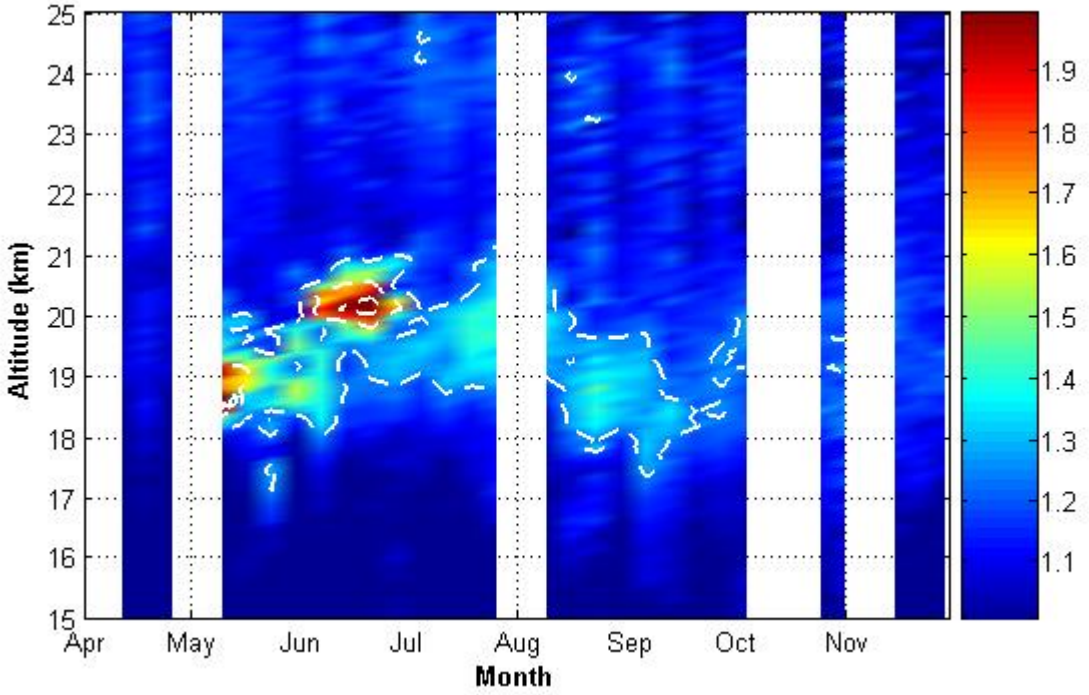

b)

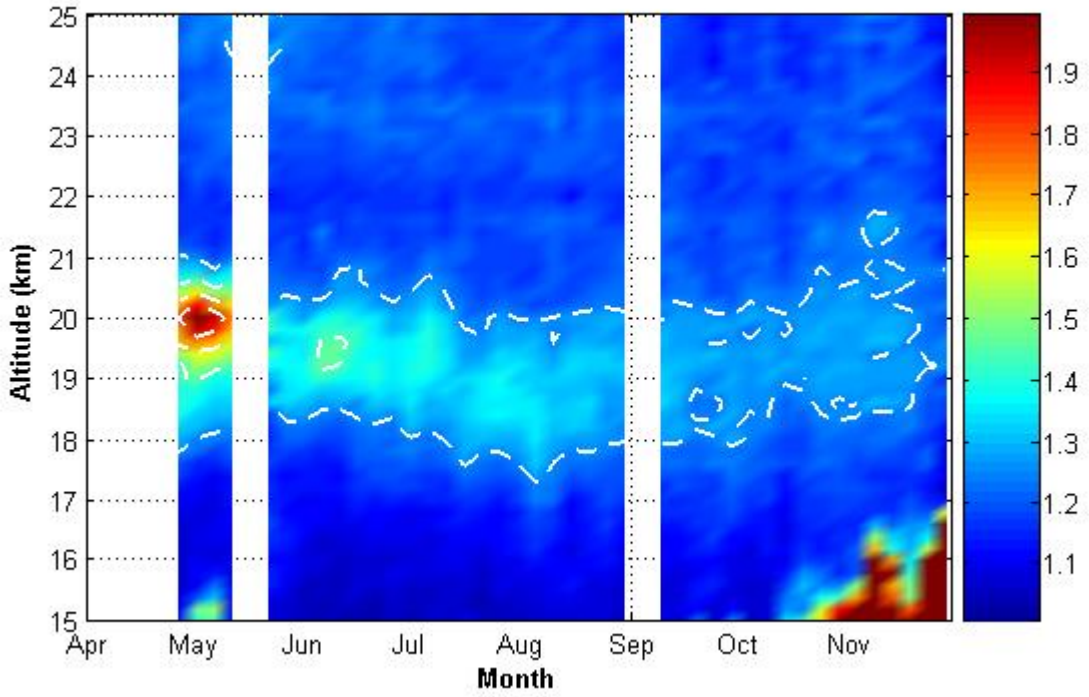

Figure 8 : Time series of weekly-averaged profiles of scattering ratio at 532 nm obtained from ground-based (a) and space-borne (CALIOP, b) LiDAR observations over Reunion Island between April 2015 and December 2015. The scattering ratios from CALIOP have been averaged within ± 5°in latitude and ± 50° in longitude (extending from Africa to Australia) around Reunion Island.

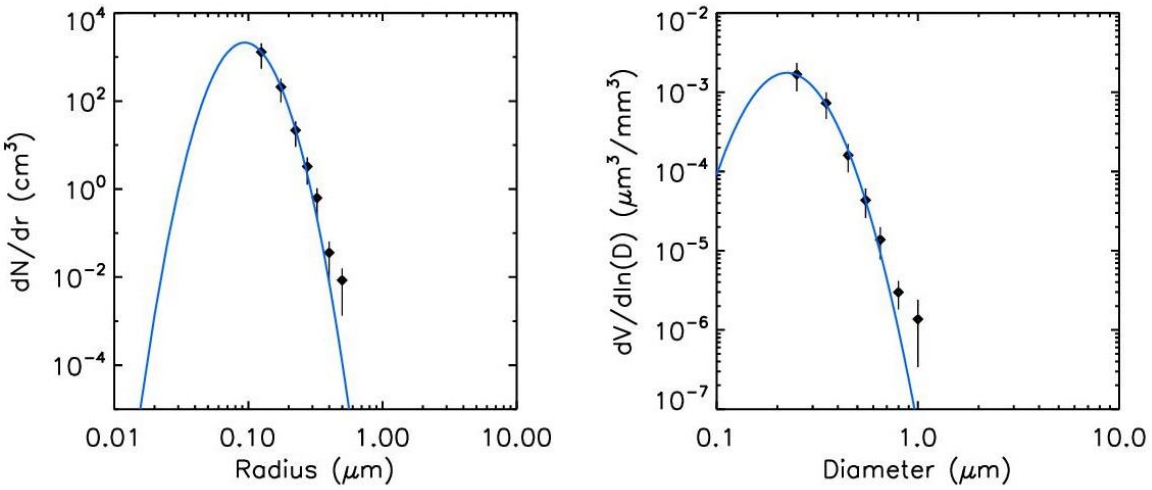

Figure 9 : Number (dN/dln(D)) and Volume concentration (dV/dln(D)) obtained from LOAC OPC observations on 19 May 2015 at 1746 UTC over the Reunion site.

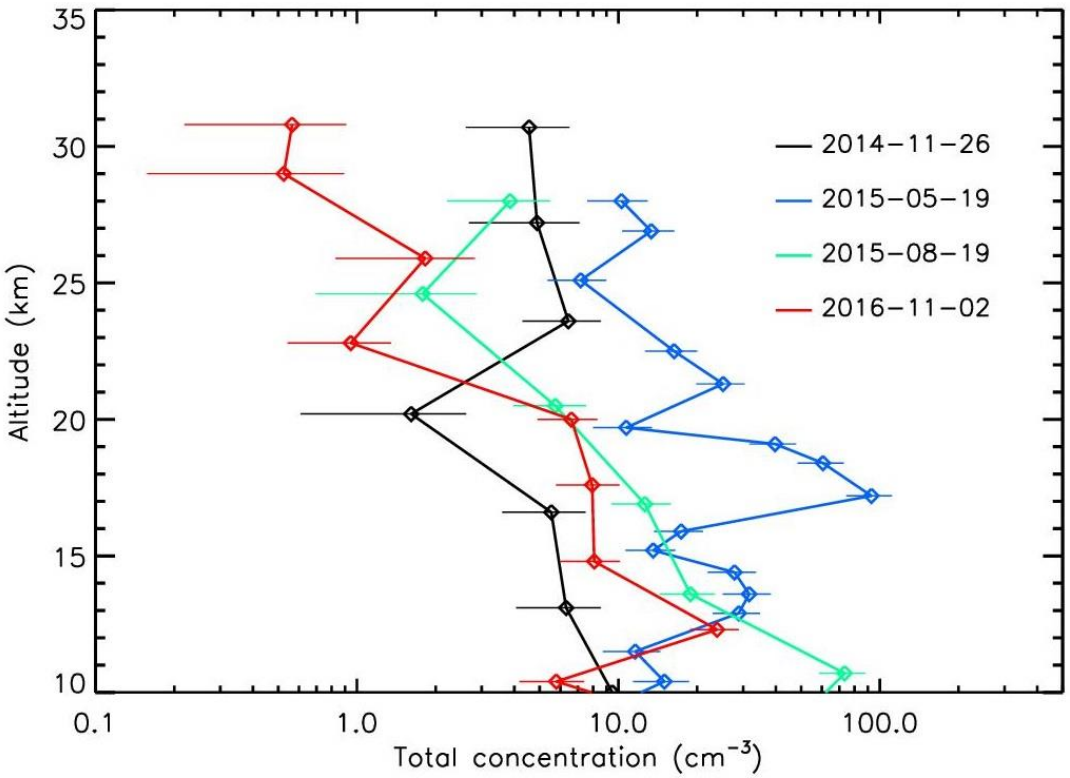

Figure 10 : Total number concentration of aerosols (0.2-50µm) profiles obtained from LOAC OPC observations over Reunion during the 26 November 2014 (black line), the 19 May 2015 (blue line), the 19 August 2015 (green line) and the 2 November 2016 (red line).

a)

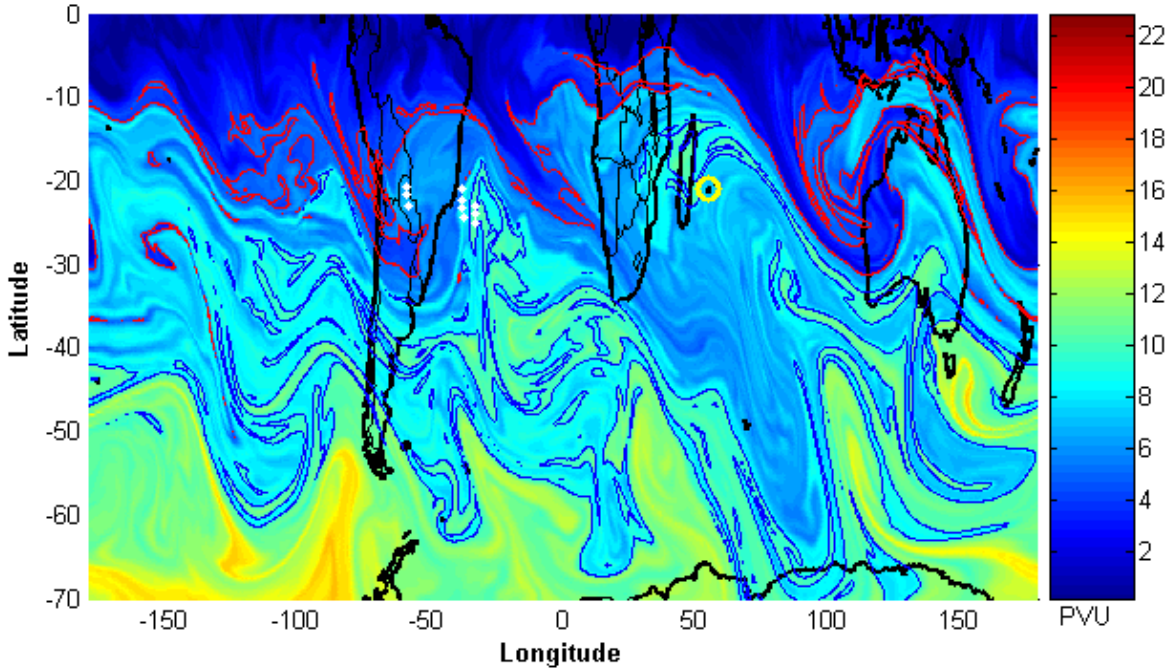

b)

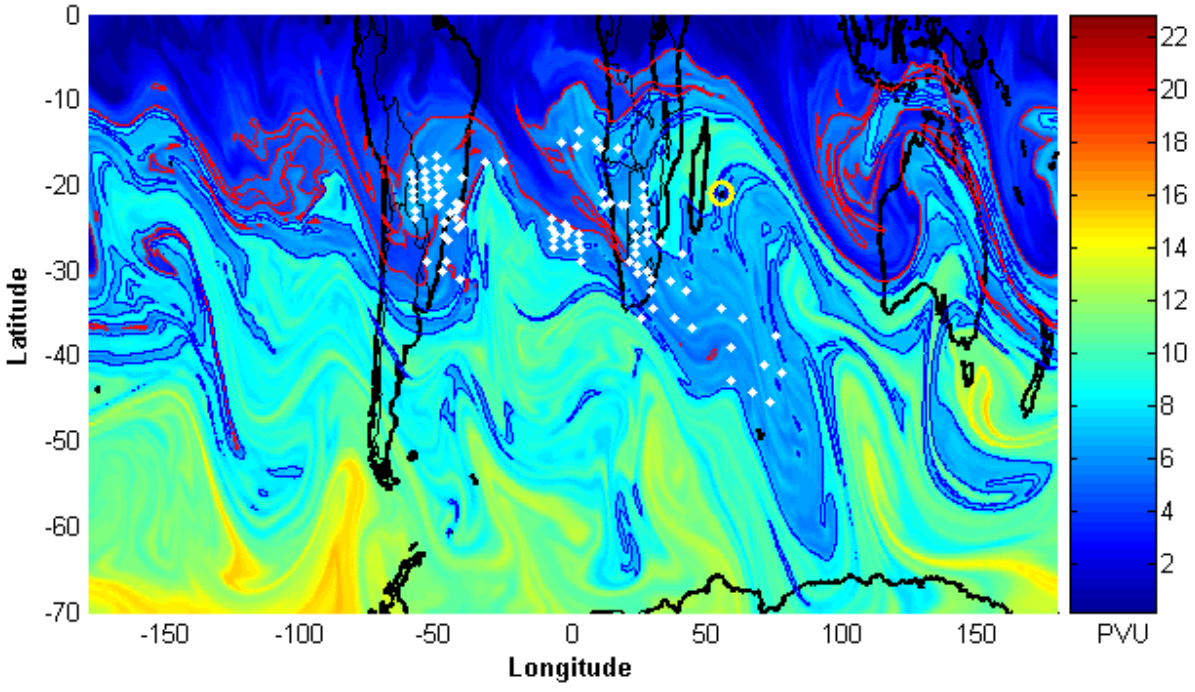

Figure 11 : Advected PV map at the 400 K level obtained from the MIMOSA model (a) on 27 April 2015 and (b) on 01 May 2015. The positions of the subtropical barrier (red line) and a south dynamical barrier (blue line) are detected from the DyBAL code. The white dots represent the localization of the aerosol plume at 400 K ± 5 K obtained from OMPS observations, while the yellow circles indicate the Reunion site.

a)

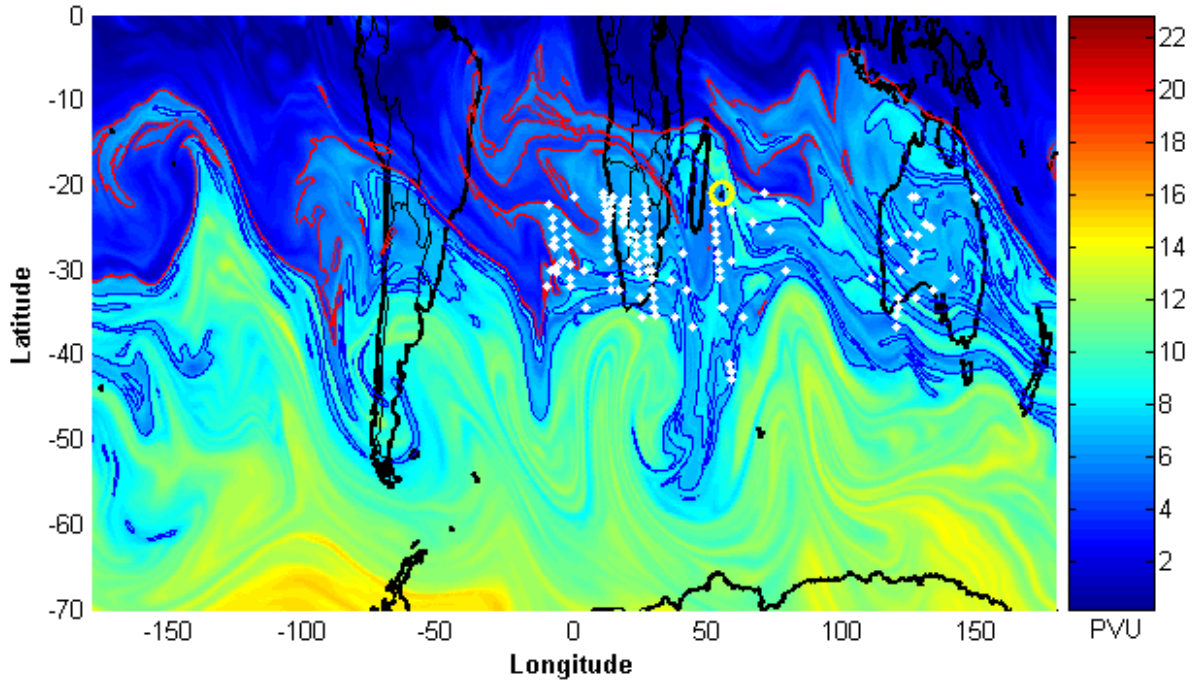

b)

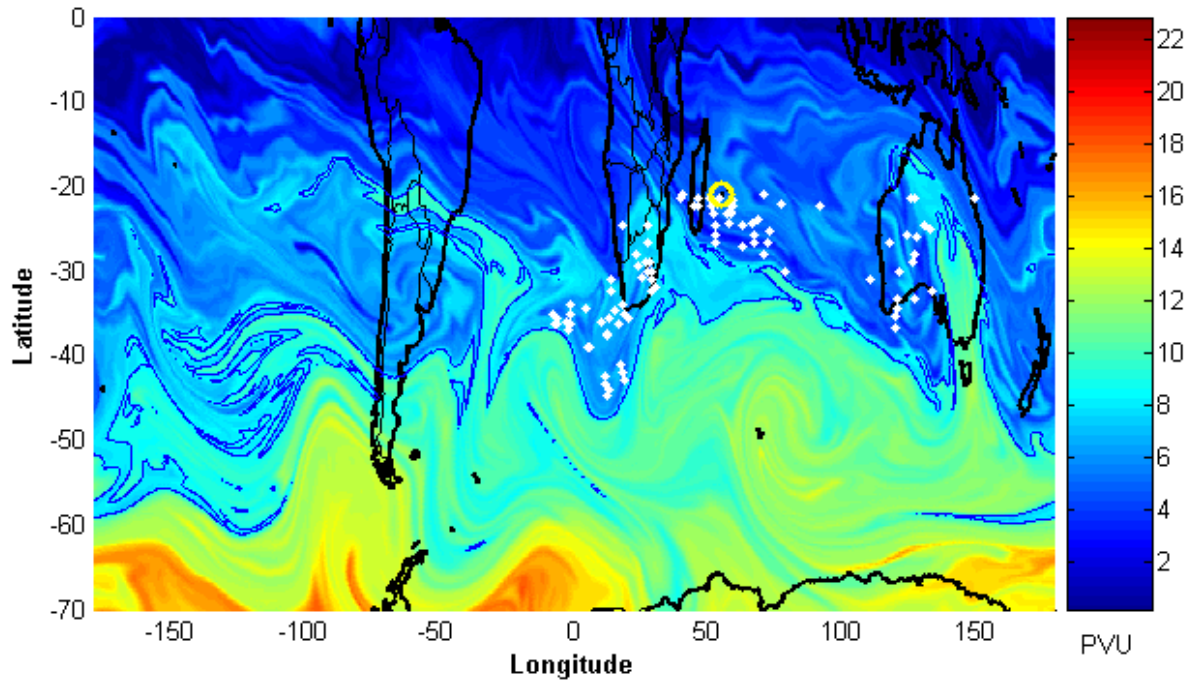

Figure 12: Same as Figure 11 but for (a) 19 May 2015 and (b) 03 June 2015.